Effect of Brownian Forces and Hydrodynamic Interactions on Colloids in Confined Flows

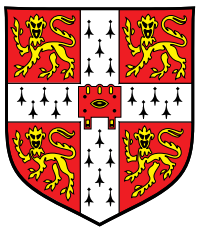

Jimaan Sane
Queens' College
University of Cambridge

A thesis submitted in partial fulfilment of the requirements for the Certificate of Postgraduate Studies in Theoretical Chemistry.
Easter 2005

Contents

Declaration

This dissertation describes research carried out in the Department of Chemistry from the Michaelmas Term 2004 to the Easter Term 2005. Unless otherwise indicated, the research described is my own and not the product of collaboration.

1 Introduction

The main purpose of this project is to test the applicability of Stochastic Rotation Dynamics (SRD) for the study of confined flows of suspended particles. Because SRD includes both Brownian and hydrodynamic forces, it is particularly well suited for the study of dispersion phenomena. We therefore choose to test it by simulating Taylor diffusion for colloidal particles. Taylor's original arguments assumed tracer particles, whereas if the size of the suspended particles is no longer negligible compared to the size of the pores they are transported through, there should be substantial corrections to Taylor's predictions. In particular when the channel becomes so narrow that particles cannot diffuse past each other – the case of one-dimensional diffusion – we expect to find important differences. This should have applications to flow in porous media.

Particle based methods like SRD have advantages over traditional continuum methods because complex boundary conditions are much easier to implement. It is therefore easier to simulate particle laden flows. Moreover, interactions between the particles can be added in a straightforward manner, so that aggregation processes under confined flow conditions can be studied. These have many potential applications in industry (e.g. asphaltenes in heavy oils etc...). Such applications are the longer term goals of my PhD, but first we must develop and test the method, which is the goal of this CPGS report.

In §2 we review some basic fluid dynamics. In §3 we describe the case of two particles sedimenting in solution, and study what happens when Brownian motion is added to the classic solution by Brenner[3]. §4 presents SRD and we discuss our choice of simulation parameters. §5 gives an account of the effects of walls on the self diffusion of colloidal particles. §6 explains Taylor diffusion solutes and §7 shows the corrections to the dispersion introduced by finite size of colloids, as demonstrated by Brenner & Edwards[18]. In §8 we describe one-dimensional diffusion and §9 gives an overview of an experiment carried out to investigate laning at high Reynolds.

2 Basic Fluid Dynamics

We will begin by giving a brief overview of some basic fluid dynamics and show how the main equations of motion are derived.

2.1 The Navier-Stokes Equations

Fluid flows are usually described by the velocity $\mathbf{u} = \mathbf{u}(x,t)$ at any point x and time t. In Cartesian coordinates, the velocity field can be written in terms of the components u, v and w

$$u = u(x,y,z,t),\ v = v(x,y,z,t),\ w = w(x,y,z,t). \tag{1}$$

It is often useful to view the flow as streamlines. These are defined as curves along which the velocity is parallel to the local velocity at any given time.

The rate of change of any given quantity (say f) at a fixed point of the flow is $\partial f/\partial t$. In contrast, the rate of change of f, as would be measured by an observed moving with flow as Df/Dt and is given by

$$\frac{Df}{Dt} = \frac{d}{dt} f[x(t), y(t), z(t), t] \tag{2}$$

where $x(t)$, $y(t)$ and $z(t)$ give the local velocity field

$$dx/dt = u,\ dy/dt = v\ , dz/dt = w. \tag{3}$$

Using the chain rule, (2) can be written as

$$\frac{Df}{Dt} = \frac{\partial f}{\partial x}\frac{dx}{dt} + \frac{\partial f}{\partial y}\frac{dy}{dt} + \frac{\partial f}{\partial z}\frac{dz}{dt} + \frac{\partial f}{\partial t}, \tag{4}$$

such that

$$\frac{Df}{Dt} = \frac{\partial f}{\partial t} + \frac{\partial f}{\partial x}u + \frac{\partial f}{\partial y}v + \frac{\partial f}{\partial z}w. \tag{5}$$

It follows that

$$\frac{Df}{Dt} = \frac{\partial f}{\partial t} + (\mathbf{u}\cdot\nabla)\mathbf{f}. \tag{6}$$

The operator D/Dt is called the Lagrangian derivative and describes the rate of change with time measured by an observed moving with the fluid. This should be distinguished from the local Eulerian derivative $\partial f/\partial t$ which measures change relative to a fixed position.

The principle of conservation of mass requires that the rate of change of a mass of fluid contained within a certain volume V must equal the outflow through its boundaries ∂V

$$\frac{d}{dt}\int_V \rho dV = -\int_{\partial V} \rho\mathbf{u}\cdot\mathbf{n}dS \tag{7}$$

where dV and dS are the differential operators for volume and surface and $\mathbf{n}$ the outward normal to the boundary. Applying the divergence theorem and the fact that V is fixed we obtain

$$\int_V \frac{\partial\rho}{\partial t}dV = -\int_V \nabla\cdot(\rho\mathbf{u})dV. \tag{8}$$

Equating the integrands yields the conservation of mass equation

$$\frac{\partial\rho}{\partial t} + \nabla\cdot(\rho\mathbf{u}) = 0 \tag{9}$$

or

$$\frac{D\rho}{Dt} + \rho\nabla\cdot\mathbf{u} = 0. \tag{10}$$

When the density of the fluid particles does not change with time, the fluid is said to be imcompressibe and $\nabla \cdot \mathbf{u}$=0.

The stress τ is defined as the force per unit area acting across a surface of fluid. Balancing the forces on an infinitesimally small volume shows that τ is linearly related to the surface normal $\mathbf{n}$ by $\tau = \sigma \cdot \mathbf{n}$ where σ is the stress tensor.

The rate of change of the momentum acting on V is due to the outflow of momentum through the boundary and to the forces acting on the surface (like pressure or friction) and on the volume (like gravity)

$$\frac{d}{dt}\int_V \rho \mathbf{u} dV = -\underbrace{\int_{\partial V} (\rho \mathbf{u})\mathbf{u}\cdot\mathbf{n} dS}_{\text{momentum flux}} + \underbrace{\int_V \mathbf{f} dV}_{\text{body forces}} + \underbrace{\int_{\partial V} \sigma\cdot\mathbf{n} dS}_{\text{surface forces}} . \qquad (11)$$

By using the divergence theorem again and equating the integrals, we arrive at

$$\rho\frac{D\mathbf{u}}{Dt} + \mathbf{u}\left(\frac{\partial\rho}{\partial t} + \nabla\cdot(\rho\mathbf{u})\right) = \mathbf{f} + \nabla\cdot\sigma \qquad (12)$$

The second term is zero from the conservation of mass principle so the momentum equation now reads

$$\rho\frac{D\mathbf{u}}{Dt} = \mathbf{f} + \nabla\cdot\sigma. \qquad (13)$$

The stress tensor is shown to be symmetric ($\sigma = \sigma^T$) by applying the conservation rule to angular momentum. We define the strain-rate tensor $\mathbf{e}$ as the symmetric part $\frac{1}{2}(\nabla u + (\nabla u)^T)$ of the velocity gradient. If the fluid is incompressible and Newtonian[1] then the stress tensor can be rearranged as

$$\sigma = -p\mathbf{I} + 2\eta\mathbf{e} \qquad (14)$$

where p is the pressure, η the viscosity and $\mathbf{I}$ the identity matrix. Combining (14) & (13) gives

$$\rho\frac{D\mathbf{u}}{Dt} = -\nabla p + \eta\nabla^2\mathbf{u} + \mathbf{f} \qquad (15)$$

$$\nabla\cdot\mathbf{u} = 0. \qquad (16)$$

where ∇^2 denotes the Laplace operator $\frac{\partial^2}{\partial x^2} + \frac{\partial^2}{\partial y^2} + \frac{\partial^2}{\partial z^2}$. These equations are know as the Navier-Stokes equations and govern the motion of fluids. Due to their non linearity, solutions to these equations are generally hard to find. Only in a few special cases such as for the Stokes equations has this been done exactly.

[1] A Newtonian fluid is characterised by the fact that application of a shear stress produces a flow with constant shear strain. This induced strain is proportional to the applied stress and the constant of proportionality η is the viscosity

2.2 The Stokes Equations

Let U and L denote the characteristic speed and length scale of the flow. The expression of the coordinates in terms of the dimensionless coordinates are

$$\mathbf{r} = L\tilde{\mathbf{r}}\ ,\ \mathbf{u} = U\tilde{\mathbf{u}} \tag{17}$$

where the tilde indicates a dimensionless quantity. It follows that

$$t = \frac{U}{L}\tilde{t} = T\tilde{t}\ ,\ p = \frac{\eta U}{L}\tilde{p} = P\tilde{p} \tag{18}$$

where T and P indicate the scales for time and pressure. Scaling the derivatives yields $\frac{\partial}{\partial t} = \frac{1\tilde{\partial}}{T\partial t}$ and $\nabla = \frac{1}{L}\tilde{\nabla}$. Upon substituting into the Navier-Stokes equations, rearranging and dropping the tildes, we obtain

$$Re\left(\frac{\partial \mathbf{u}}{\partial t} + (\mathbf{u}\cdot\nabla)\mathbf{u}\right) = -\nabla p + \nabla^2\mathbf{u}. \tag{19}$$

We define

$$Re = \frac{\rho U L}{\eta} \tag{20}$$

as the dimensionless Reynolds number. We can see that for $Re \ll 1$, the viscous term $\tilde{\nabla}^2\tilde{u}$ will dominate and for $Re \gg 1$, inertia $((\tilde{u}.\tilde{\nabla})\tilde{u})$ will be more important. The Reynolds number is thus of particular importance as it can give a rough indication of the relative magnitude of two key terms in the Navier-Stokes equation[1]. The case of steady 'very viscous' flow with very small Reynolds number ($Re \ll 1$), involves the omission of the inertial terms compared to viscous terms resulting in the so-called creeping motion equations or Stokes equations

$$\begin{aligned} \nabla\cdot\sigma = \nabla^2\mathbf{u} - \frac{1}{\eta}\nabla p &= -\mathbf{f} \\ \nabla\cdot\mathbf{u} &= 0 \end{aligned} \tag{21}$$

where $\mathbf{f}$ denotes the force applied on the fluid. As there is no longer a $\partial/\partial t$ term in the equation, the force is proportional to the velocity and not $\partial\mathbf{u}/\partial t$. The absence of inertia means the fluid particles have no 'memory'. The flow is solely governed by the current boundary conditions and applied forces and responds to changes instantaneously. If all the forces were abruptly removed, the fluid would stop flowing outright. The Stokes equations are linear too, so solutions for a given geometry can be superimposed. Stokes flow is also said to be reversible. It is so well ordered that if all forces are reversed then the particles will retrace their paths exactly. For example, this is the reason why particles sedimenting under Stokes flow *cannot* move relative to each other. If the spheres were flowing towards each other for instance then all the forces were suddenly reversed, the spheres would sediment away from each other, not describing the same motion.

2.3 Extension to Flow Between Plates : Plane Poiseuille Flow

In real systems, the flow is often surrounded by boundaries that can affect the motion. It is thus useful to have solution for such cases. The simplest example of bounded flow is flow between parallel plates. If we assume flow in the x direction only, the velocity is independent of x and the Stokes equations reduce to the scalar form

$$\frac{d^2u}{dy^2} = \frac{\rho g}{\eta}. \tag{22}$$

We have written the pressure difference as $dp/dx = \rho g$ where ρ is the fluid density and g the applied field. A flow with this velocity distribution is know as a plane Poiseuille flow.

It has been observed that viscous fluids have no-slip (stick) boundary conditions. The components of the velocity field of the fluid must equal those of the boundary. If the boundary is at rest then $u = 0$ at the boundary. For parallel plates separated by a distance $h = 2a_p$, the boundary conditions are $u(0) = u(h) = 0$. Integrating the Stokes equations in two dimensions and implementing the boundary conditions yields

$$u = \frac{\rho g}{2\eta} y(h-y). \tag{23}$$

The average velocity across the plates is given by

$$\bar{u} = \frac{1}{2a_p}\int_0^{a_p} u dy \tag{24}$$

and can be rearranged in terms of a_p and u such that

$$u = \frac{3}{2}\bar{u}\left(1 - \frac{y^2}{a_p^2}\right). \tag{25}$$

3 Particles in a Fluid Under Gravity: Sedimentation

If an isolated hard sphere of radius a is dropped in a fluid, it accelerates under gravity until the drag force F_s described by Stokes' law balances the gravitational force F_g and it attains terminal velocity U_s, known as the Stokes velocity. If g is the strength of the gravitational field and the spheres' density differs from that of the liquid by $\triangle\rho$. U_s is found by balancing the forces acting on the sphere

$$\left.\begin{array}{l} F_s = 6\pi\eta a U_s \\ F_g = \frac{4}{3}\pi a^3 \triangle\rho g \end{array}\right\} U_s = \frac{2a^2\triangle\rho g}{9\eta}.$$

Note that in two dimensions, balancing the forces acting on a disk yields

$$\left.\begin{array}{l} F_s = 6\pi\eta a U_s \\ F_g = \pi a^2 \triangle\rho g \end{array}\right\} U_s = \frac{a\triangle\rho g}{6\eta}.$$

The sedimenting sphere sets up a velocity field $\mathbf{u}$ in the fluid. The derivation of $\mathbf{u}$ consists of two steps. First we show an example of general solution to the Stokes' equation and then an application of that solution to a sphere.

3.1 Example of a General Solution to Stokes Equation

Papkovic & Neuber[4] derived an exact solution to the Stokes Equations. Here is a brief outline of their proof.

By rewriting the pressure $p = \nabla^2\Pi$ in terms of a scalar Π and substituting into the Stokes equation we obtain $\nabla^2(\eta\mathbf{u} - \nabla\Pi) = 0$. For reasons that will become apparent later, we further introduce the harmonic vector Φ such that $\eta\mathbf{u} = \nabla\Pi - \Phi$. Substituting this expression for the velocity into the incompressibility equation, we further obtain $\nabla^2\Pi = \nabla\cdot\Phi$. Integrating yields $\Pi = \frac{1}{2}(\mathbf{x}\cdot\Phi + \chi)$ with $\nabla^2\chi = 0$.

Thus in the absence of body forces, any Stokes flow can be written in terms of a harmonic vector Φ and a harmonic scalar χ

$$2\eta\mathbf{u} = \nabla(\chi + \mathbf{x}\cdot\phi) - 2\Phi \text{ and } p = \nabla\cdot\Phi.$$

It is sometimes possible to find a harmonic scalar ϕ such that $\chi = \mathbf{u}.\nabla\phi - \mathbf{2}\phi$. If so, we can dispense with χ in the above equation by replacing Φ by $\Phi' = \Phi + \nabla\phi$ (we can do so because Φ' is harmonic[2]). Any Stokes flow can thus be written in terms of a harmonic vector Φ and a harmonic scalar χ

$$2\eta\mathbf{u} = \nabla(\chi + \mathbf{x}\cdot\ \Phi\ ) - 2\ \Phi \ \text{ and } \ p = \nabla\cdot\Phi.$$

3.2 Solution for a Sphere Under Stokes flow

Oseen then extended the problem to a sphere in a Stokes flow[2]. The field is modelled by a point force acting on its centre. The problem is written as

$$\nabla\cdot\sigma \equiv \eta\nabla^2\mathbf{u} - \nabla p = -\mathbf{f}\delta(\mathbf{x}) \quad (26)$$

$$\nabla\cdot\mathbf{u} = 0. \quad (27)$$

His derivation is as follows: We now assume the solution holds for a harmonic function of the form $\Phi = \alpha\mathbf{f}/r$. By substituting Φ into the expression derived by Papkovic & Neuber, we arrive at[3]

$$2\eta\mathbf{u} = \frac{-\alpha\mathbf{f}}{r}\left(\mathbf{I} + \frac{\mathbf{xx}}{r^2}\right). \quad (28)$$

Utilising (14) we also obtain the following expression for the stress

$$\sigma = 3\alpha\frac{\mathbf{xx}(\mathbf{x}.\mathbf{f})}{r^5}. \quad (29)$$

On the surface of a hard sphere immersed in a viscous fluid, $r = R$, $\mathbf{n} = \mathbf{x}/R$ and

$$\mathbf{u}\cdot\mathbf{n} = \frac{-\alpha\mathbf{f}\cdot\mathbf{n}}{\eta R} \text{ and } \sigma\cdot\mathbf{n} = 3\alpha\frac{\mathbf{n}(\mathbf{n}\cdot\mathbf{f})}{R^2}. \quad (30)$$

[2] Proof of this can be found in the appendix.

[3] Recall $\nabla\mathbf{x} = \mathbf{I}$, $\nabla r = \frac{\mathbf{x}}{r}$ and $\nabla f(r) = f'(r)\nabla r = f'(r)\frac{\mathbf{x}}{r}$. Hence $\nabla\left(\frac{1}{r}\right) = -\frac{\mathbf{x}}{r^3}$ and $\nabla\nabla\left(\frac{1}{r}\right) = -\frac{\mathbf{I}}{r^3} + 3\frac{\mathbf{xx}}{r^5}$.

The force acting on the surface of the sphere is

$$\mathbf{f} = -\int_{r=R} \sigma \cdot \mathbf{n} dS = -3\alpha \mathbf{f} \cdot \left(\int \mathbf{nn} \frac{dS}{R^2} = \frac{4\pi}{3} \mathbf{I} \right) \tag{31}$$

such that α must satisfy the condition $\alpha = -1/4\pi$.

Using (28), the velocity field set up in the fluid by the sedimenting sphere now reads

$$\mathbf{u} = \mathbf{f}\mathbf{J}(\mathbf{x}) \text{ where } \mathbf{J}(\mathbf{x}) = \frac{1}{8\pi\eta r} \left(\mathbf{I} + \frac{\mathbf{xx}}{r^2} \right) \tag{32}$$

where $\mathbf{J}(\mathbf{x})$ is known as the Oseen tensor. When all the forces are balanced, $F_s = F_g$ the velocity field set up by the sphere reads

$$\mathbf{u} = F_s \mathbf{J}(\mathbf{x}) = \frac{3a}{4r} U_s \left(\mathbf{I} + \frac{\mathbf{xx}}{r^2} \right). \tag{33}$$

and decays as $1/r$.

3.3 Effect of a Second Particle

We now wish to study the effect of a second sphere. We assume the particles are close enough to interact hydrodynamically and that they are sedimenting in an unbounded fluid. To find a solution to this two particle problem, we use the method of reflections. The method decomposes the velocity and pressure into a sum of linear terms and uses successive iterations whereby each term must satisfy the boundary conditions associated with the particles.

The method of reflections was first introduced by Smoluchowski(1911) and was treated at length by Happel & Brenner for the case of sedimenting spheres[3]. The method is presented below.

The appropriate boundary conditions for any sphere (say a) translating through an unbounded fluid which is at rest at infinity are

$$\mathbf{u} = \mathbf{u}_a \text{ on } a \tag{34}$$

$$\mathbf{u} \rightarrow 0 \text{ as } r \rightarrow \infty \tag{35}$$

and the local fluid motion is assumed to satisfy the Stokes equations. Given that the equations of motion and boundary conditions are linear, the local velocity and pressure fields may be decomposed into a sum a fields, namely

$$\mathbf{u} = \mathbf{u}^{(1)} + \mathbf{u}^{(2)} + \mathbf{u}^{(3)} + \mathbf{u}^{(4)} + \ldots \tag{36}$$

$$\mathbf{p} = \mathbf{p}^{(1)} + \mathbf{p}^{(2)} + \mathbf{p}^{(3)} + \mathbf{p}^{(4)} + \ldots \tag{37}$$

each term of which separately satisfies the equations of motion and vanishes at infinity. Again because of linearity we may further subdivide each of these into a finite sum of terms also satisfying the the governing equations and vanishing at

infinity. Focusing on particle a, we define the field $\mathbf{u}^{(1)}$ such that it satisfies the boundary conditions on a and decays as $1/r$ away from a i.e.

$$\mathbf{u}^{(1)} = \mathbf{u}_a \text{ on } a. \tag{38}$$

At the boundary of any other sphere in the system (say b), the boundary condition is then defined as

$$\mathbf{u}^{(1)} + \mathbf{u}^{(2)} = \mathbf{u}_b \text{ on } b, \tag{39}$$

termed as the 'reflection' of the field $\mathbf{u}^{(1)}$ from particle b, where $\mathbf{u}^{(1)}$ and $\mathbf{u}^{(2)}$ are the local values of the velocity fields. Now $\mathbf{u}^{(2)}$ will in turn decay as $1/r$ away from b such that

$$\mathbf{u}^{(3)} = -\mathbf{u}^{(2)} \text{ on } a, \tag{40}$$

termed as the 'reflection' of the field $\mathbf{u}^{(2)}$ from particle a. In order to complete the approximation for the entire fluid field it is necessary to establish $\mathbf{u}^{(3)}$ in the vicinity of b also. An approximation of the field is now available for a system of two spheres in an unbounded fluid, and is given by $\mathbf{u} = \mathbf{u}^{(1)} + \mathbf{u}^{(3)}$. This reflection process may be continued as many times as necessary to obtain satisfaction of all boundary conditions to the desired accuracy. The force $\mathbf{f}_a$ exerted on the particle by the fluid is then obtained by summing the drag contributions of the individual fields such that

$$\mathbf{f}_a = \mathbf{f}_a^{(1)} + \mathbf{f}_a^{(3)} + \mathbf{f}_a^{(5)} + \ldots \tag{41}$$

where $\mathbf{f}_a^{(j)}$ is the force on a associated with the jth reflection. It is convenient to choose an axis (the z axis say) of the reference system of coordinates along a line connecting the centres of the two particles, and we will assume they only move in a plane (zx). We denote l the distance separating the centre of the two spheres of radii. We recall that the boundary conditions to be satisfied are

$$\begin{aligned}
\mathbf{u}^{(1)} &= \mathbf{u}_a \text{ on } a && (42)\\
\mathbf{u}^{(2)} &= -\mathbf{u}^{(1)} + \mathbf{u}_b \text{ on } b && (43)\\
\mathbf{u}^{(3)} &= -\mathbf{u}^{(2)} \text{ on } a && (44)\\
\mathbf{u}^{(4)} &= -\mathbf{u}^{(3)} \text{ on } b, \text{ etc.} && (45)
\end{aligned}$$

The force exerted by the fluid on a is

$$\mathbf{f}_a^{(1)} = -\mu K_a \mathbf{u}_a = -\mu K_a \left(\mathbf{i} U_{ax} + \mathbf{k} U_{az}\right) \tag{46}$$

which correctly indicates that it is anti parallel to the velocity vector. Note that $K_a = 6\pi\mu a$ is the resistance coefficient for a hard sphere. We compute the translational effect from a by assuming it generates the same field as would be produced by a point force situated at the centre of the particle and so from (32) we can express $\mathbf{u}^{(1)}$ as

$$\mathbf{u}^{(1)} = \frac{K_a U_{ax}}{8\pi r}\left(\mathbf{i} + \mathbf{r}\frac{x}{r^2}\right) + \frac{K_a U_{az}}{8\pi r}\left(\mathbf{k} + \mathbf{r}\frac{x}{r^2}\right) \tag{47}$$

where r is the distance measured from the centre of a. The centre of b has the coordinates $x = 0$, $y = 0$, $z = l$ such that the value of $\mathbf{u}^{(1)}$ at this point is

$$[\mathbf{u}^{(1)}]_b = \frac{K_a}{8\pi l}\left(\mathbf{i}U_{ax} + 2\mathbf{k}U_{az}\right). \tag{48}$$

From which we can compute the force exerted on b

$$\begin{aligned}\mathbf{f}_b^{(2)} &= -\mu K_b(U_b - [\mathbf{u}^{(1)}]_b) \\ &= -\mathbf{i}\mu K_b\left(U_{bx} - \frac{K_a U_{ax}}{8\pi l}\right) - \mathbf{k}\mu K_b\left(U_{bz} - \frac{K_a U_{az}}{4\pi l}\right).\end{aligned} \tag{49}$$

Similarly we can compute the velocity field generated by $\mathbf{f}_b^{(2)}$ acting on b. Note that in this case the coordinate system will be at the centre of b such that

$$[\mathbf{u}^{(2)}]_a = \mathbf{i}\frac{K_b}{8\pi l}\left(U_{bx} - \frac{K_a U_{ax}}{8\pi l}\right) - \mathbf{k}\frac{K_b}{4\pi l}\left(U_{bz} - \frac{K_a U_{az}}{4\pi l}\right). \tag{50}$$

Using this result we can compute $\mathbf{f}_a^{(3)}$ and find that

$$\begin{aligned}\mathbf{f}_a^{(3)} &= \mu K_a[\mathbf{u}^{(2)}]_a \\ &= \mathbf{i}\frac{\mu K_b K_a}{8\pi l}\left(U_{bx} - \frac{K_a U_{ax}}{8\pi l}\right) - \mathbf{k}\frac{\mu K_b K_a}{4\pi l}\left(U_{bz} - \frac{K_a U_{az}}{4\pi l}\right).\end{aligned} \tag{51}$$

Similarly,

$$\begin{aligned}\mathbf{f}_a^{(5)} &= \mathbf{i}\mu K_a\left(\frac{K_a}{8\pi l}\right)\left(\frac{K_b}{8\pi l}\right)^2\left(U_{bx} - \frac{K_a U_{ax}}{8\pi l}\right) \\ &+ \mathbf{k}\mu K_a\left(\frac{K_a}{4\pi l}\right)\left(\frac{K_b}{4\pi l}\right)^2\left(U_{bz} - \frac{K_a U_{az}}{8\pi l}\right).\end{aligned} \tag{52}$$

Thus, upon summation we obtain

$$\begin{aligned}\mathbf{f}_a &= \mathbf{f}_a^{(1)} + \mathbf{f}_a^{(3)} + \mathbf{f}_a^{(5)} + \ldots \\ &= -\mathbf{i}\mu K_a\left(U_{ax} - \frac{K_b}{8\pi l}\left(U_{bx} - \frac{K_a U_{ax}}{8\pi l}\right) \times \left[1 + \left(\frac{K_a}{8\pi l}\right)\left(\frac{K_b}{8\pi l}\right) + \left(\frac{K_a}{8\pi l}\right)^2\left(\frac{K_b}{8\pi l}\right)^2 + \ldots\right]\right) \\ &\quad -\mathbf{k}\mu K_a\left(U_{az} - \frac{K_b}{4\pi l}\left(U_{bz} - \frac{K_a U_{az}}{8\pi l}\right) \times \left[1 + \left(\frac{K_a}{4\pi l}\right)\left(\frac{K_b}{4\pi l}\right) + \left(\frac{K_a}{4\pi l}\right)^2\left(\frac{K_b}{4\pi l}\right)^2 + \ldots\right]\right)\end{aligned}$$

Expressing the geometric series as a fraction and combining terms, we find

$$\frac{\mathbf{f}_a}{\mu K_a} = -\mathbf{i}\frac{U_{ax} - (K_b U_{bx}/8\pi l)}{1 - (K_a K_b)/(8\pi l)^2} - \mathbf{k}\frac{U_{az} - (K_b U_{bz}/4\pi l)}{1 - (K_a K_b)/(4\pi l)^2}. \tag{53}$$

Note that $\mathbf{f}_b$ can be obtained by interchanging the subscripts a and b in the above equation.

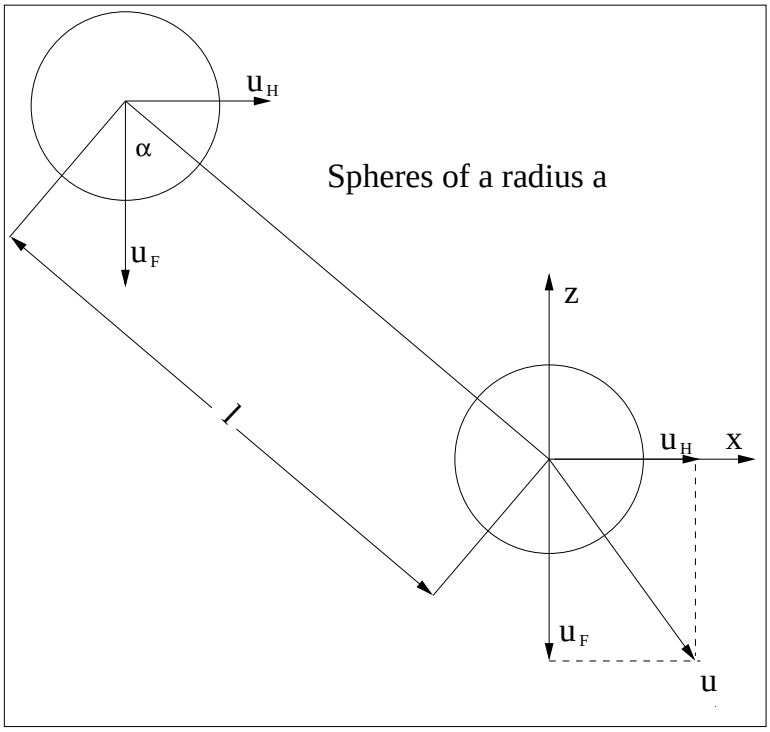

Figure 1: Coordinate system for the two particle interaction

In the case of equal-size spheres, as shown in Fig1, (53) reduces to

$$-\frac{\mathbf{f}}{6\pi\mu a} = \mathbf{i}\frac{U_X}{1+(3/4)(a/l)} + \mathbf{k}\frac{U_Z}{1+(3/2)(a/l)}. \tag{54}$$

where a is the radius of the sphere. The fluid exerts the same force on both spheres such that their motion is parallel with the same velocity. As a result they will always maintain the same distance between each other.

If α is the angle gravity makes with the line of centres, and the absolute value of the gravitational field F is defined, we can find expressions for the velocity in the direction of gravity U_F and for the velocity of drift in the horizontal direction. We begin by recalling that

$$U_F = U_X \cos\alpha + U_Z \sin\alpha \tag{55}$$

where

$$U_X = \frac{-F\sin\alpha}{6\pi\mu a}\left(1+\frac{3a}{4l}\right),\ U_Z = \frac{-F\cos\alpha}{6\pi\mu a}\left(1+\frac{3a}{2l}\right). \tag{56}$$

By combining these relationships we obtain

$$U_F = U_S\left(1+\frac{3a}{4l}(1+\cos^2\alpha)\right). \tag{57}$$

Similarly

$$U_H = U_S\frac{3a}{4l}\sin\alpha\cos\alpha \tag{58}$$

and the fall velocity satisfies $U = \sqrt{U_F^2 + U_H^2}$.

Drift will thus only occur when the angle $\alpha \neq 0$ or 90^o, that is, when the spheres are not falling one behind each other along their line of centres, or side by side perpendicular to their line of centres. The fall velocity will be at its minimum in the latter case. when they are closer together (Fig.2). As mentioned earlier sedimenting spheres have no relative motion. Consequently, if they fall with a drift they will appear to be chasing each other.

As it is assumed all hydrodynamic interactions are instantaneous, the Schmidt number $Sc = \eta/\rho D_s$, [4] which represents the relative velocity with which momentum diffuses across, is assumed to be infinite also.

3.4 Brownian Motion

So far, we have seen that two particles fall faster when falling close to each other, and along their line of centres. However, all the analysis up to now has been carried out ignoring Brownian effects. When examining dilute suspensions of colloidal spheres in water or some liquid, one notices that each particle moves about with a continuous but random jiggling motion. We can think of these particles as being

[4] D_s denotes the diffusion constant of the solvent particles.

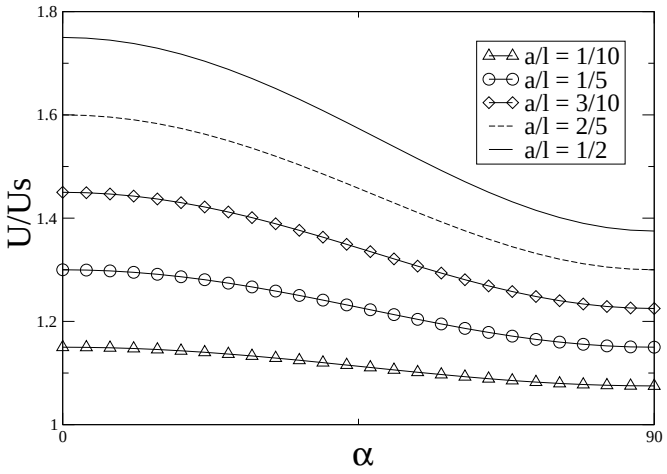

Figure 2: Normalised fall velocity $\frac{U}{U_s} = \sqrt{\left(\frac{U_E}{U_S}\right)^2 + \left(\frac{U_H}{U_S}\right)^2}$ for different values of the angle gravity makes with their line of centres (α), and the relative distance between their centres (a/l). The fall velocity is normalised by U_S, the Stokes velocity for an isolated particle sedimenting in an unbounded fluid.

constantly bombarded by random impacts of the molecules of the liquid. The resulting motion of the colloids is known as Brownian motion[8], which sees them diffuse relative to one another. In order to interpret this diffusive spreading, it can be useful to model their behaviour using random walks. This involves allowing each particle to take a step (δx say) in any (equally probable) direction along each axis every time-step δt. The motions in each of these directions are statistically independent as the colloids upon colliding with the water molecules will 'lose' memory of their initial velocity. The particles will thus move independently from one another such that the walk will not be biased. We expect the behaviour of the colloids to be different in the case of sedimentation when Brownian effects are taken into consideration. In contrast to pure Stokes flow, the particles now move relative to each other such that l is no longer fixed.

The particles' positions are updated as

$$\begin{pmatrix} x_i(t) \\ z_i(t) \end{pmatrix} \rightarrow \begin{pmatrix} x_i(t+\delta t) = x_i(t) \pm \triangle x_i(t) \\ z_i(t+\delta t) = z_i(t) \pm \triangle z_i(t). \end{pmatrix}$$

The spreading of a particle undergoing a random walk can be measured by the mean squared distance traversed in a time t

$$< x^2 >=< z^2 >= 2Dt \tag{59}$$

where D denotes the diffusion constant of each particle. For particles diffusing relative to each other, we expect the relative diffusion constant to be twice the standard diffusion constant as each particle is undergoing its own random walk. The particles' relative mean squared displacement along the x-axis is thus given by

$$< x_{rel}^2 >=< (x_i - x_j)^2 >=< x_i^2 > + < x_j^2 > - \underbrace{2 < x_i x_j >}_{0} = 2D_{rel}t \tag{60}$$

where $D_{rel} = 2D$ is the relative diffusion constant. We can relate this relative displacement to l and α by

$$l = \sqrt{x_{rel}^2 + z_{rel}^2}\ ,\ \cos\alpha = \frac{z_{rel}}{\sqrt{x_{rel}^2 + z_{rel}^2}}\ ,\ \sin\alpha = \frac{x_{rel}}{\sqrt{x_{rel}^2 + z_{rel}^2}}, \tag{61}$$

such that

$$\begin{aligned} \frac{U}{U_S} &= \sqrt{\left(\frac{U_F}{U_S}\right)^2 + \left(\frac{U_H}{U_S}\right)^2} \\ &= \sqrt{\left(1 + \frac{3a}{4\sqrt{x_{rel}^2 + z_{rel}^2}}\left(1 + \frac{z_{rel}^2}{x_{rel}^2 + z_{rel}^2}\right)\right)^2 + \left(\frac{3a}{4\sqrt{x_{rel}^2 + z_{rel}^2}}\frac{x_{rel}^2 z_{rel}^2}{x_{rel}^2 + z_{rel}^2}\right)^2} \\ &= f(x_{rel}, z_{rel}) \end{aligned} \tag{62}$$

The probability that the particles have diffused a distance $r = l$ from each other at any given time is

$$P(r) = P(x_{rel})P(z_{rel}) = \frac{1}{4\pi D_{rel} t} e^{-(x_{rel}^2 + z_{rel}^2)/4D_{rel}t} \tag{63}$$

from which we can see that larger diffusion constants will render flatter distribution functions. The average fall velocity, which takes into account Brownian effects now reads

$$< \frac{U}{U_s} >= \int\int P(x_{rel})P(z_{rel})\, f(x_{rel}, z_{rel}). \tag{64}$$

3.4.1 Simulation and Results

We performed a simple simulation to see the evolution of (64). This was done using the inbuilt Gaussian distribution function in Matlab. Results are shown in Fig.3.

As expected the inclusion of diffusion causes a temporal evolution in the relative fall velocity. The normalised fall velocity decays to the Stokes velocity with time. This means the velocity of each particle tends to the velocity of an isolated particle implying the particles are diffusing away from one another and gradually no longer feel each others' presence.

As the particles now move relative to each other, the angle their line of centres makes with gravity now changes randomly. While they remain close enough to influence each other they will be seen to still follow each other and the 'direction' along which they fall will keep changing randomly.

The results are scaled with the Stokes time $t_s = a/U_s$ and the diffusion time $t_b = a^2/D$. They indicate the time a particle takes to sediment or diffuse a distance equal to its own radius. These timescales are significant as they give an indication of how the particles are behaving relative to each other. The non dimensional Peclet number is given by their ratio

$$Pe = \frac{t_d}{t_s}. \tag{65}$$

For example $Pe = 5$ implies $t_d = 5t_s$ which indicates that by the time a particle has sedimented a distance equal to five times its radius, it has diffused a distance equal to once its radius. The Peclet number thus indicates the amount of diffusion; the higher its value, the slower the diffusion. Their relative motion is therefore reduced and we would expect their relative fall velocity to decay to the Stokes velocity less rapidly.

Fig.3(top) shows the decay of a particles normalised velocity with $Pe = 5$. For larger Peclet numbers, the decay would be slower while for smaller Peclet numbers the normalised velocity would decay much faster. Fig.3(bottom) shows that when time is normalised by the diffusion time t_d, all curves eventually collapse to a master curve. This illustrates the fact that the normalised fall velocity evolves on the same timescale as diffusion. After $10t_b$, there is still a correction to the

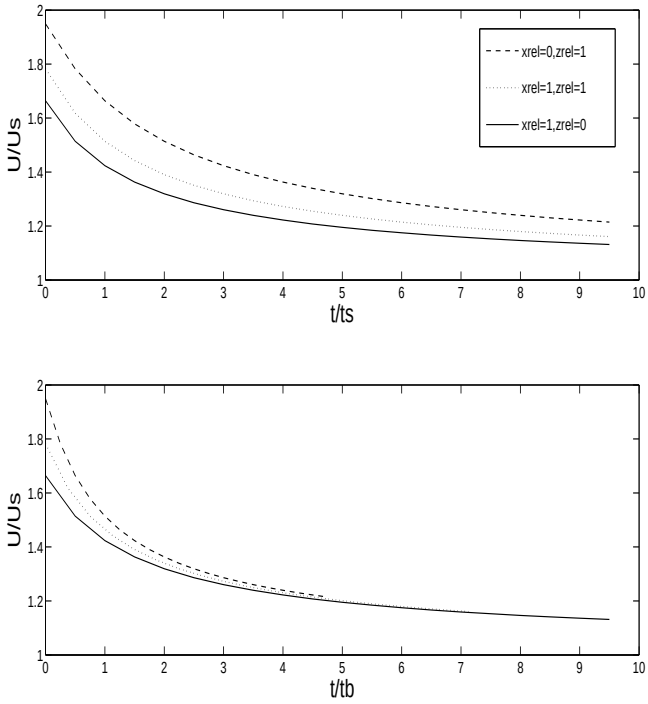

Figure 3: Temporal evolution of the normalised average fall velocity $< \frac{U}{U_s} >= \int\int P(x_{rel})P(z_{rel})f(x_{rel},z_{rel})$ plotted for different initial startup positions x_{rel} and z_{rel}. The new expression for the fall velocity now incorporates effects of Brownian motion and is plotted as a function of time normalised by the Stokes time t_s and the diffusion time t_d.

Stokes velocity of around 10%. The decay gets increasingly slow with time as diffusion scales as $\sim \sqrt{t}$. Note that Fig.3(top) is Peclet number dependent, whereas Fig.3(bottom) is Peclet number independent.

The relative fall velocity also gives a measure of the effect of a secondary particle and therefore gives an indication as to level of correlation in the particles' motion. The time their motion will be correlated therefore depends on the amount of diffusion the particles will undergo as they are sedimenting, and thus on the Peclet number *Pe*.

Note that we have assumed Brownian motion only occurred in two dimension. In three dimensions, we would also include the y-component of the relative distance between the spheres y_{rel}, such that $r = \sqrt{x_{rel}^2 + y_{rel}^2 + z_{rel}^2}$ and $P(r) = P(x_{rel})P(y_{rel})P(z_{rel})$. We do not expect to see qualitatively significant changes but further work will include analysis in three dimensions.

4 Stochastic Rotation Dynamics

As we have seen, Brownian forces should not be neglected when looking at sedimentation. To study the effect of diffusion on more complex systems, we make use of Stochastic Rotation Dynamics (SRD). The SRD model, which was first introduced by Malenavets & Kapral [5], is in the spirit of lattice gas models. It has the advantage of easily being coupled to a solute, such as polymers or colloids which can subsequently be treated using molecular dynamics algorithms. SRD provides a novel way of treating hydrodynamics problems with Brownian effects.

The solvent is modelled by an ensemble of particles whose positions ($r_i(t)$) are updated by successive streaming and collision procedures. During the streaming step, the particles are allowed to propagate for a given time δt_c, after which their positions are updated via

$$r_i(t+\delta t_c) = r_i(t) + v_i(t)\delta t_c \tag{66}$$

where $v_i(t)$ is the velocity of the particles. The collision step (which occurs every δt_c) involves splitting the particles into small cells and the velocity of each particle within a cell (v_{cell}) is rotated relative to the centre of mass velocity of the cell,

$$v_i(t+\delta t_c) = v_{cell}(t) + \omega \cdot (v_i(t) - v_{cell}(t)) \tag{67}$$

where ω denotes a rotation matrix which rotates the particles by an angle $\pm\alpha$ with equal probability. The collision procedure transfers momentum between the fluid particles while conserving the total momentum of each cell.

The fluid particles only interact with one another through the collision procedure. Direct interactions between the solvent particles are not taken into account. This coarse graining step is the main cause of the efficiency of simulations using SRD. This carefully constructed rotation procedure ensures energy and momentum are conserved locally, thus capturing the properties of the Navier-Stokes equations. The Brownian behaviour of the fluid particles is included by assigning each particle with a random velocity drawn from a Maxwell type distribution.

The system is coupled to a thermostat to prevent any significant fluctuations in the average temperature. This can arise when an external field is applied for example. The thermostat acts by rescaling the relative velocities (i.e. the velocity of a fluid particle relative to the centre of mass velocity) when the local temperature deviates from the desired temperature.

Kikuchi*et.al.*[6] calculated analytical expressions for the viscosity $\eta = \eta_{kin} + \eta_{col}$, resulting from contributions of the streaming and collision steps respectively in 2 dimensions

$$\eta_{kin} = \frac{\gamma k_B T \delta t_c}{a_0^2}\left(\frac{\gamma}{(\gamma - 1 + e^{-\gamma})(1-\cos\alpha)} - \frac{1}{2}\right) \tag{68}$$

$$\eta_{col} = \frac{m(1-\cos\alpha)}{6\delta t_c}(\gamma - 1 + e^{-\gamma}) \tag{69}$$

where γ is the number of solvent particles per cell, m the mass of a fluid particle.

Colloids of mass M can be embedded in the solvent if we wish to simulate the behaviour of spherical colloids in a fluid. They are propagated through the Velocity Verlet algorithm with the molecular dynamic time step δt

$$R_i(t+\delta t) = R_i(t) + V_i(t)\delta t + \frac{F_i(t)}{M}\delta t^2 \quad (70)$$

$$V_i(t+\delta t) = V_i(t) + \frac{F_i(t)+F(t+\delta t)}{2M}\delta t \quad (71)$$

where R_i and V_i are the position and velocity of the colloid, and F_i the total force exerted on the colloid.

They interact with each other through a repulsive potential:

$$\varphi_{cc}(r) = \begin{cases} 4\varepsilon\left(\left(\frac{\sigma_{cc}}{r}\right)^{48} - \left(\frac{\sigma_{cc}}{r}\right)^{12} + \frac{1}{4}\right) & (r \le 2^{1/24}\sigma_{cc}) \\ 0 & (r \ge 2^{1/24}\sigma_{cc}) \end{cases}$$

while the interaction between the colloid and the solvent is described by the less precipitous potential:

$$\varphi_{cs}(r) = \begin{cases} 4\varepsilon\left(\left(\frac{\sigma_{cs}}{r}\right)^{12} - \left(\frac{\sigma_{cs}}{r}\right)^{6} + \frac{1}{4}\right) & (r \le 2^{1/6}\sigma_{cs}) \\ 0 & (r \ge 2^{1/6}\sigma_{cs}) \end{cases}$$

where the L-J repulsive strength is chosen usually chosen to be $\varepsilon = 2.5k_BT$. We choose smaller exponents to describe the latter potential as both the mass and range of the colloid-fluid interaction are less than that of the colloid-colloid interaction. The colloid-colloid potential enables colloids to be modelled as hard spheres while allowing accurate integration of the Verlet equations for relatively large timesteps δt. Although exponents in the potential are chosen such that it is as large as possible, $\varphi_{cc}(r)$ is constrained by the fact that δt is limited by the colloid-fluid interaction, and not the colloid-colloid interaction.

When the density of the solvent particles n_s is much higher than that of the colloids, even small overlaps between two colloids can lead to large attractive forces. Louis*et.al.*[7] showed that for low enough colloid densities, the equilibrium depletion interaction between two colloids is given by

$$\Phi_{depl}(d) = n_s k_B T \left[V_{excl}(d) - V_{excl}(\infty)\right], \quad (72)$$

where $V_{excl}(d)$ is the free volume excluded to the solvent by the overlap. Unwanted depletion forces can be counterbalanced by introducing compensating interactions $\Phi_{comp} = -\Phi_{depl}$.

4.1 Simulation Parameters

We now explain the motivation behind our choice of SRD parameters.

Simulation units for mass and unit cell size were set as $m = m_s = 1$, $a_0 = 1$ and $k_B T = 1$. The program units for time and velocity are be related to real units via

$$\left.\begin{array}{l} [k_B T] = \frac{ML^2}{T^2} \\ [m] = M \\ [a_0] = L \end{array}\right\} [time] = a_0 \sqrt{\frac{m}{k_B T}}$$

and

$$[vel] = \frac{L}{[time]} = \sqrt{\frac{k_B T}{m}}. \tag{73}$$

In order to eliminate depletion, it can prove useful to simulate colloids with a slightly smaller hydrodynamic core. Accordingly, we set the colloid-solvent interaction range to be slightly less the colloid half diameter σ_{cc}. We further we chose ε such that the colloid-colloid potential $\varepsilon(d) = \varepsilon$ at distances $d = 2\sigma_{cs}$, and that at that distance d, depletion interactions have just become zero. This ensure there are never too few solvent particles between two colloids thus avoiding any depletion forces.

As mentioned earlier, the molecular dynamic timestep δt is limited by the colloid-solvent interaction. We do not want the potential φ_{cs} to ever become too large and consequently wish to construct a fairly conservative timestep. The former is achieved by preventing any individual solvent molecule from approaching too close to σ_{cs}. It will only interact with the colloid particle beyond the cutoff range $2^{1/6}\sigma_{cs}$ so we would like for an SRD particle to travel a distance equal to $1/5$ of the distance $\sigma_{cs}(2^{1/6} - 1)$ for a given timestep at most. SRD particles each have an average velocity $c_F = \sqrt{\frac{k_B T}{m}}$ and hence an appropriate value of δt should satisfy

$$c_F = \frac{\sigma_{cs}(2^{1/6} - 1)}{5\delta t} \Rightarrow \delta t = \sigma_{cs}(2^{1/6} - 1)/5c_F. \tag{74}$$

This leads to values in the order of $\delta t = 0.1 a_0 (m_s/k_B T)^{1/2}$ when $\sigma_{cs} = 2a_0$. Using the same arguments, we can compare this timestep with the one we would construct if we were simulating standard Brownian motion. Brownian motion is scale invariant; the random walk does not depend on the size mean free path. The Brownian timestep is henceforth constrained by the colloid-colloid interaction only. Likewise, we desire colloids to travel $1/5$ of the distance $\sigma_{cc}(2^{1/24} - 1)$ at each Brownian timestep such that

$$< x^2 >= 2D\delta t_b = \frac{(\sigma_{cc}(2^{1/24} - 1))^2}{25} \Rightarrow \delta t_b = \frac{(\sigma_{cc}(2^{1/24} - 1))^2}{50D}. \tag{75}$$

Using analytical expressions such as that derived by Kikuchi*et.al.*[6] we can calculate the self diffusion constant D of the fluid and predict that the ratio of the SRD to Brownian timesteps is $\delta t_b/\delta t \sim 0.12$.

To ensure the motion is liquid like, care must be taken in picking the SRD collision interval δt_c such that the Schmidt number $Sc = \nu/D_s = \frac{k_B T \nu \delta t_c}{m} \gg 1$, where

$\nu = \eta_s/\rho_s$ is the kinematic viscosity of the solvent. We choose a relatively small collision interval ($\delta t_c = 4\delta t$) leading to $Sc \sim 5$.

The current version of the SRD code does not yet implement stick boundary conditions on the colloids such that it experiences drag force with coefficient $\xi = 4\pi\nu a$ (instead of 6). In real suspension the value is much closer to 6 and so changing the boundary condition should give slightly more accurate results, although we do not expect the changes to be qualitatively significant.

Under plane Poiseuille flow, between parallel plates separated by a distance $h = 2a$, the fluid and the colloids usually travel with mean velocities $\bar{v} = \frac{2}{3}v_{max} \pm \triangle v$. v_{max} is the velocity at the midpoint between the plates and can be predicted by integrating the Stokes equations and utilising the boundary conditions for Poiseuille flow $v_{max} = \frac{\rho g a^2}{2\eta}$. The field applied on the solvent g is usually chosen such that $v_{max} \ll c_F = \sqrt{2k_BT/m_f}$, where c_F denotes the speed of sound in the fluid. Typically, we choose g such that the Mach number is bounded by $Ma = \bar{v}/c_F \sim 0.1$.

To avoid inertial effects, the Reynolds number must be kept relatively. Drawing attention to the fact that for small collision intervals the collisional part of the viscoscity term dominates ($\eta \sim \eta_{col}$), and that $\eta \sim \gamma$, the Reynolds number for the flow can be shown to scale as

$$Re = \frac{\bar{v}a}{\nu} \sim \frac{\rho_s g}{2\eta}a^3 \sim g\delta t_c^2 a^3. \tag{76}$$

This quantity therefore only depends on the field applied on the solvent and the width of the channel only.

The density of colloids is chosen to more or less match that of the solvent ($\rho_c = \gamma$) in order to avoid any sedimentation. We define the Peclet number of a colloid $Pe_c = Pe(\sigma_{cc}/2a)$. Given that the colloid self diffusion constant scales as $D_{col} \sim \eta^{-1}$, Pe_c can also be shown to scale as

$$Pe_c = \frac{\bar{v}\sigma_{cc}}{2D_{col}} \sim \frac{\rho g \sigma_{cc}}{4\eta}a^2\eta \sim \gamma g \sigma_{cc} a^2, \tag{77}$$

i.e. the colloid Peclet number depends on the average number of fluid particles per unit cell, the gravitational field, the size of the colloid and the width of the channel.

These approximations are very useful as they enable us to efficiently tune the properties of the system from the outset.

5 Diffusion in a Pipe without Flow

5.1 Diffusion and the Velocity Autocorrelation Function

As stated earlier, a hard sphere of radius a_c sedimenting with velocity U in an unbounded fluid experiences a drag force $F = 6\pi\eta a_c U$. If the sphere also undergoes Brownian diffusion, the characteristic diffusion coefficient for the motion is given by the Stokes-Einstein relation[8]

$$D = \frac{k_BT}{6\pi\eta a_c}. \tag{78}$$

According to Newton's law, a particle's mass m_c multiplied by its acceleration dv/dt, where v is its velocity, equals the sum of all forces acting upon it. From these principles, we can write the equation of motion for a particle undergoing Brownian motion as[8]

$$m\frac{dv}{dt} = f(t) - \xi v \tag{79}$$

known as the *Langevin equation*. In this model representation, two forces act on the particle; friction described by Stokes' law with the drag coefficient $\xi = 6\pi\eta a_c$, and a random force due to the Brownian motion $f(t)$.

The Langevin model can further be used to illustrate the idea of the time correlation function[9]. Here are the main arguments:

The velocity autocorrelation function reveals how quickly a particle forgets its initially velocity due to Brownian fluctuations and is constructed by first multiplying the velocity of a particle at time $t = 0$ with its subsequent velocity at time t and then averaging the product over many collisions to get the time correlation function $C(t) = \langle v(0)v(t)\rangle$.

An expression for the velocity autocorrelation function is obtained by manipulating the Langevin equation appropriately. We first point out that the direction of the Brownian force is uncorrelated to the particle velocity, we may write $\langle v(0)f(t)\rangle = \langle v(0)\rangle\langle f(t)\rangle$. Also, as the Brownian force is random, it will on average by equal to zero over many realisations ($\langle f(t) = 0\rangle$).

By multiplying both sides of the equation by $v(0)$, taking the ensemble average and utilising the statements above, it is shown that

$$\langle v(0)v(t)\rangle = \langle v^2(0)\rangle e^{-\xi t/m}. \tag{80}$$

Since $\langle v^2(0)\rangle = \langle k_b T/m\rangle$, the above equation can be rewritten as

$$\langle v(0)v(t)\rangle = \frac{k_B T}{m} e^{-\xi t/m}, \tag{81}$$

i.e. the function decays exponentially with time. This is only true for short times however. At longer times[5], the correlation function has been shown[10] to follow the well known algebraic long time tail $C(t) \sim t^{d/2}$ where d is the dimensionality of the system. Ignoring the tail and integrating the velocity autocorrelation function gives

$$\int_0^\infty \langle v(0)v(t)\rangle = \frac{k_B T}{m}\int_0^\infty e^{-\xi t/m}dt = \frac{k_B T}{\xi} = D, \tag{82}$$

because $\int_0^\infty e^{-\xi t/m}dt = m/\xi$. In the two dimensional geometry, the longtime tail of the correlation function goes as $1/t$ so that the integral diverges logarithmically, suggesting that the self diffusion coefficient remains time dependent even at long times. This is not the case in three dimensions.

The study of correlation functions is thus useful as their integrals are related to transport coefficients.

[5]Here we mean long on the hydrodynamic timescale

5.2 Wall effects

In this section, we turn our attentions to the motion of a colloidal particle in a confined geometry. It is well documented that a sphere suspended in a fluid at rest next to a flat wall is subject to hydrodynamic effects due to the sphere-wall interaction.

Happel & Brenner[3] showed that the effect of containing walls was in many ways analogous to the effect of a secondary particle, and could be accurately predicted by an extension of the method of reflections described in section 3.3. They demonstrated that when a sphere got closer to a wall, the Stokes drag force acting on it increased, and that its diffusion coefficient was therefore smaller than in the bulk. For this reason, the effect of a tube wall is to slow down the motion of a particle travelling in its vicinity.

In three dimensions, the drag force acting on a sphere can be separated into independent components due to the linearity of the Stokes equations, for motion parallel and perpendicular to the wall

$$F_{\parallel} = F\zeta_{\parallel} \tag{83}$$
$$F_{\perp} = F\zeta_{\perp} \tag{84}$$

and consequently, the diffusion constants for motion parallel and perpendicular to the wall are

$$D_{\parallel} = \zeta_{\parallel}^{-1} D \tag{85}$$
$$D_{\perp} = \zeta_{\perp}^{-1} D, \tag{86}$$

where $\zeta_{(\parallel,\perp)}$ is the appropriate correction factor due to the presence of the wall. Furthermore, even in the low Reynolds number limit, the exact solutions for the effective wall drag force do not have a closed analytical form. Approximate representations for $\zeta_{(\parallel,\perp)}$ can be obtained using the method of reflections and to first order are given by [3]

$$\zeta_{\parallel}^{-1} = \frac{D_{\parallel}}{D} \sim 1 - \frac{9}{16}\frac{a_c}{x} + O\left(\frac{a_c}{x}\right)^3 \tag{87}$$
$$\zeta_{\perp}^{-1} = \frac{D_{\perp}}{D} \sim 1 - \frac{9}{8}\frac{a_c}{x} + O\left(\frac{a_c}{x}\right)^3, \tag{88}$$

where x is the distance from the centre of the sphere to the wall.

The method of reflections nonetheless fails to provide an exact analytical solution for the drag force acting on a sphere when a second wall is present. In their simplest form, approximate analyses based on the linearity of the Stokes' equations, have assumed the effects of the drag from each wall could be independently superimposed[3].

Due the friction exerted by the walls, the long time tail of the velocity correlation will also be lost as expected. In their theoretical study of a particle suspended in a fluid between two parallel plates, Bocquet and Barrat[11] showed that this was

indeed the case. In the two dimensional case, the integral of the velocity correlation function in a bounded fluid will no longer diverge as the algebraic tail sinks at long times. The sink in the algebraic tail occurs at a time T, dependent on the width of the channel h. The diffusion constant thus evolves as $D \sim \int_0^T 1/t \sim \log(h)$.

5.3 Simulation and Results

Simulations were performed in SRD to illustrate wall effects. All simulations were performed in two dimensions. Colloidal particles were represented as disks of the same radius in a fluid bounded by infinitely thin parallel plates and in the bulk. No external field was applied and the particle was allowed to diffuse freely.

Fig.4 shows the evolution of the self diffusion coefficients for the motion of a disk like particle in a quiescent fluid. Only the case of motion parallel with respect to the boundary was considered. We see that, as expected, the diffusion coefficient does not converge in the bulk. In the case of diffusion in a narrow channel, the diffusion constant reached a maximum, before eventually saturating at a slightly lower value. The velocity autocorrelation function is plotted in the inset. In an unbounded fluid, the function is always positive. We see that in the presence of walls it becomes negative but a longtime tail is recovered at long times. These features have also been observed in other computational studies[12].

In Fig.5, we show the particle diffusion constant for channels of different sizes. We see that within the error bars, the evolution is consistent with $D \sim \log(h)$. We observe rapid fluctuations for narrower channels. The increase becomes less important as the duct becomes larger. No study of the drag coefficients has been reported in two dimensions. We will in future studies carry out simulations in three dimensions to determine the correction factor for the drag due to the wall, and check whether we can get good agreement with the theoretical values predicted by Happel & Brenner.

Fig.6 shows that, at first glance, collisions with the wall (circled) seem to cause a reversal in the diffusion to a certain extent. This correlation (if any)may be down to hydrodynamic effects due to the particle being very close to the wall. The low density of fluid particles between the colloid and the wall may also render measurements difficult. We will address these points in more depth in future studies.

6 Flow in a Pipe with Diffusion: Taylor Diffusion

Taylor diffusion is the result of convection due to a flow and molecular dispersion, as first studied by G.I Taylor [13]. When a coloured solute is injected into a channel of liquid flowing under a Poiseuille flow, it initially gets stretched out into a paraboloid type slug by the velocity distribution. Convection alone contributes to this early axial spreading. Radial diffusion subsequently causes the deformed concentration profile to even out, as particles at the front of the paraboloid migrate onto streamlines closer to the edges, and particles at the rear diffuse inwards onto

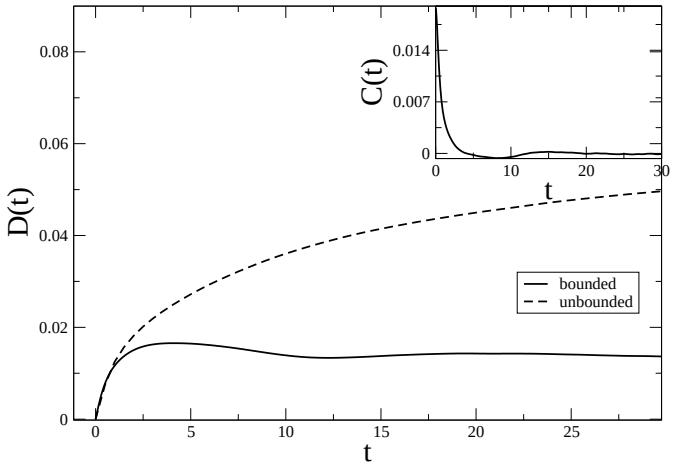

Figure 4: Parallel (x) component of the self diffusion coefficient of a disk like particle (D_{col}) of radius $a = 2.15a_0$ relative to the orientation of the channel, in a bounded and unbounded fluid respectively. The particle is initially located at the midpoint between two walls separated by a distance $h = 12a_0$. The fluid is at rest and is simulated with $\gamma = 5$ SRD particles per unit cell. The inset shows a plot of the particle's velocity autocorrelation function and illustrates the recovery of the long time tail.

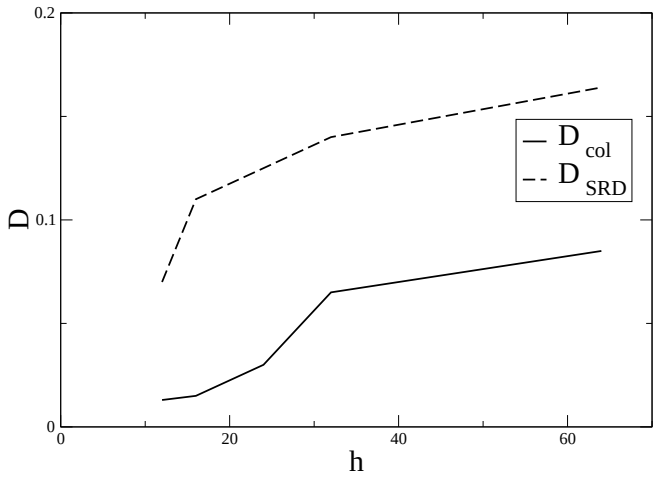

Figure 5: x-component of the self diffusion coefficient of a disk like colloidal particle of radius $a = 2.15a_0$ in channels of increasing width $h = 2a_p$. The evolution of the solvent diffusion coefficient (D_s) is also shown.

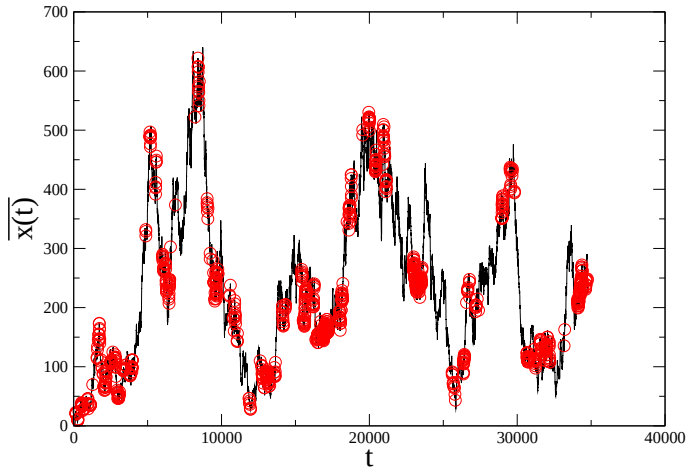

Figure 6: Parallel component of the displacement. The collisions with the wall are circled.

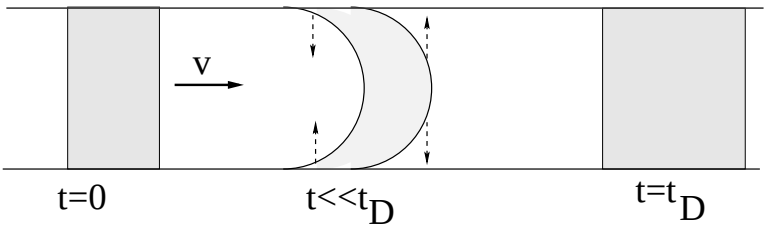

Figure 7: Taylor dispersion between parallel plates. Neglecting radial diffusion, the initial solute gets stretched to a paraboloid shaped plug. Diffusion, indicated by the vertical arrows, evens out the concentration profile leading to a wider plug.

the faster velocity streamlines. This in effect slows down the front of the slug and causes the rear to speed up, resulting in a more elongated region of the solute with a Gaussian like concentration profile.

6.1 Taylor Dispersion of Small Solutes

To get a better physical understanding of Taylor diffusion, lets assume that convection and diffusion can occur successively[14]. Convection initially stretches the solute into a parabola. The solute at front end of the parabola leads the solute at the edges by a distance $u_0 t$ after a time t. Here $u_0 = \frac{3}{2}\bar{u}$ denotes the velocity in the centre of the pipe. Diffusion across the channel then smears the parabola into a plug, as shown in Fig.7. This occurs at times $t_D \sim a_p^2/D$ it takes the solute to reach the the edges. On such timescales, the plug has a width $W_{tD} \sim u_0 t_D = u_0 a_p^2/D$. Seeing that diffusion scale as $\sim \sqrt{t}$, after N t_b 'times', the plug is stretched by a factor of $N^{1/2}$. The plugs thus grows diffusively and its width scales as

$$\langle W^2 \rangle^{1/2} \sim N^{1/2} W_{tD} \sim \left(\frac{u_0^2 a_p^2}{D} t \right)^{1/2}. \tag{89}$$

Accordingly, in addition to molecular diffusivity D ,the solute can be seen to diffuse along the channel with an effective dispersion coefficient

$$D^* \sim \frac{u_0^2 a_p^2}{D}. \tag{90}$$

Note that the effective dispersion coefficient is inversely proportional to the molecular diffusion coefficient, which may seem counter intuitive at first glance. However, solute molecules with higher molecular diffusivities spend more time diffusing across the pipe and less time sampling particular velocity streamline thus reducing their *effective* spreading. Probstein[15] presents detailed analysis for flow in a three dimensional pipe of radius a_p that yields the prefactor

$$D^* \sim \frac{\vec{u}^2 a_p^2}{48D}. \tag{91}$$

We shall carry out analysis in a two dimensions. Simulations run faster in that geometry so arguments are easier to test. Once sufficient understanding has been gained at that level, we shall continue to three dimensions.

6.1.1 Taylors' Derivation in two Dimensions

We now present the derivation for obtaining the correct prefactor in two dimensions. Our analysis follows closely the arguments of Probstein but is adapted to take into account the two dimensional geometry.

The Convection-Diffusion Equation

The dispersion process is an example of combined convection and diffusion observed when a solute of concentration $c(y,t)$ is allowed to flow between two plates under a plane Poiseuille flow.

The convection-diffusion equation describing the evolution of the concentration is given by

$$\partial_t c + u(y)\partial_x c = D\left(\partial_x^2 c + \partial_y^2 c\right), \tag{92}$$

where D is the diffusion constant as would be observed under diffusion alone.

We scale the convection-diffusion equation by introducing the following non-dimensional constants

$$x = l_o\tilde{x},\ y = a_p\tilde{y},\ t = \frac{l_0}{\bar{u}}\tilde{t},\ u = \bar{u}\tilde{u} \tag{93}$$

where l_0 and a_p represent the characteristic lengths over which concentration changes along the x-axis and the y-axis respectively. We shall thus assume they represent the dimensions of the channel. The dimensionless equation upon dropping the tildes has the form

$$Pe\partial_t c + \underbrace{Pe\frac{a_p}{l_0}u(y)\partial_x c}_{\text{axial convection}} = \underbrace{\partial_y^2 c}_{\text{radial diffusion}} + \underbrace{\frac{a_p^2}{l_0^2}\partial_x^2 c}_{\text{axial diffusion}}. \tag{94}$$

For high Peclet numbers, the terms on the left-hand side will dominate, and we will be in the convection dominated regime. Conversely, for low Peclet number, the terms on the right-hand side will become important and diffusion will dominate. Note that because of the a_p^2/l_0^2 term, radial diffusion will set in at different conditions than axial diffusion. In the case where only radial diffusion is prominent, these coefficients will scale as

$$1 \ll \frac{l_0}{a_p} = \frac{\bar{u}t}{a_p} = \frac{\bar{u}a_p^2}{a_p D} = Pe \text{ and } Pe \ll \frac{l_0}{a_p}, \tag{95}$$

where the characteristic time for radial diffusion is $t = t_D = a_p^2/D$.

The Solution

The only change in the concentration in the axial direction will follow from convection and, we assume so axial diffusion can be neglected. It is thus useful to switch to a coordinate system in which the x-axis moves with the mean speed of the flow. We will use x' and u' to denote the moving axis and the velocity with respect to the moving axis,

$$x' = x - \bar{u}t \text{ and } u' = \frac{\bar{u}}{2}\left(1 - 3\frac{y^2}{a_p^2}\right). \tag{96}$$

Under this coordinate transformation, the convection-diffusion equation becomes

$$\partial_t c + \frac{\bar{u}}{2}\left(1 - 3\frac{y^2}{a_p^2}\right)\partial_x c = D\partial_y^2 c. \tag{97}$$

where ∂_t now denotes differentiation with respect to time at points along the moving axis. We also assume that the plates are impermeable and that there is no flux at the boundaries such that $\partial_y c = 0$ on $y = a_p$.
Taylor then made the assumption that in the moving frame, the flow was quasi-steady after long times ($t \gg a_p^2/D$), and that concentration only varies in the radial direction such that $\partial_t c \approx 0$. He then extended this assumption to say that if c were independent of x with large t, then $\partial c/\partial x'$ would be independent of r. In other words, as we move with the fluid, we would expect that after a long time the axial concentration gradient will become independent of the radial position. Consequently, $\partial_{x'} c \approx \partial_{x'} \bar{c}$ where $\bar{c}$ is the average concentration across the plates.
The equation we wish to solve for is now reduced to

$$\partial_y^2 c = \frac{\bar{u}}{2D}\left(1 - 3\frac{y^2}{a_p^2}\right)\partial_{x'} c \tag{98}$$

which can be readily integrated to give the solution

$$c = c_0 + \frac{\bar{u}a_p^2}{4D}\partial_{x'} c\left(\frac{y^2}{a_p^2} - \frac{1}{2}\frac{y^4}{a_p^4}\right) \tag{99}$$

where c_0 is the concentration at $y = 0$. The average concentration over the plate separation is given by

$$\bar{c} = \frac{1}{a_p}\int_0^{a_p} c\,dy. \tag{100}$$

Upon integration, we find

$$\bar{c} = c_0 + \frac{7}{10}\frac{\bar{u}a_p^2}{4D}\partial_{x'} c \tag{101}$$

such that we can express the concentration in terms of $\bar{c}$

$$c = \bar{c} + \frac{\bar{u}a_p^2}{4D}\left(-\frac{7}{10} + \frac{y^2}{a_p^2} - \frac{1}{2}\frac{y^4}{a_p^4}\right)\partial_{x'} c. \tag{102}$$

According to Taylor $\partial_{x'} c \approx \partial_{x'} \bar{c}$ and so, upon differentiating the above expression for c the following condition must be satisfied

$$\frac{\bar{u} a_p^2}{4D} \frac{1}{l_0} \ll 1 \;\Rightarrow\; Pe \ll \frac{4 l_0}{a_p}. \tag{103}$$

The average mass flux across the plates is

$$\bar{J} = \frac{1}{a_p} \int_0^{a_p} y dy m c u' = m a_p \int_0^1 \frac{y}{a_p} d\left(\frac{a_p}{y}\right) c u' \tag{104}$$

with m the unit mass across the plates. By replacing $\partial_{x'} c$ by $\partial_{x'} \bar{c}$ and $\bar{\rho} = m\bar{c}$ and integrating we obtain

$$\bar{J} = -D^* \partial_{x'} \bar{\rho} \;\text{ (Fick's law)} \tag{105}$$

where

$$D^* = \frac{2 a_p^2 u_0^2}{105 D} \tag{106}$$

is referred to as the Taylor dispersion coefficient.
This result is somewhat significant as it states that the average solute gets dispersed relative to a plane moving with mean velocity $\bar{u}$ as though it were being dispersed by a molecular diffusion process with a dispersion coefficient $D = D^*$.
From the conservation of mass principle we obtain

$$\rho \partial_t c = -\partial_{x'} \bar{J} \;\Rightarrow\; \partial_t \bar{c} = D^* \partial_{x'}^2 \bar{c}. \tag{107}$$

In the original rest frame, the diffusion equation is written

$$\partial_t \bar{c} + \bar{u} \partial_x \bar{c} = D^* \partial_x^2 \bar{c} \tag{108}$$

and is often termed the *Taylor dispersion equation*.
These equation are valid provided the effect of axial molecular diffusion is negligible compared with the Taylor dispersion,

$$D^* \gg D \;\Rightarrow\; Pe \gg \sqrt{105/2} \sim 7. \tag{109}$$

Combining this result with the previous constrains on *Pe*, we find that Taylor dispersion only occurs in the range

$$7 \ll Pe \ll \frac{4 l_0}{a_p}. \tag{110}$$

If the initial quantity of the substance is know, say n_0, then it can easily be shown that the dispersion relation has solution

$$\bar{c} = \frac{n_0}{\sqrt{\pi D^* t}} \exp\left(-\frac{(x - \bar{u}t)^2}{4 D^* t}\right). \tag{111}$$

Measurement of the width of the concentration profile can prove useful as it provides a way of determining self diffusion constants of colloids by experiment[16].

So far, we have assumed molecular diffusion in the axial direction to be negligible. Aris[17] showed that when this was not the case ($D^* \sim D$) the effective diffusion could be written as the sum of the molecular and the Taylor dispersion coefficients

$$D_{TA} = D^* + D. \tag{112}$$

D_{TA} is termed the Taylor-Aris dispersion coefficient.

7 Taylor Diffusion of Colloids

The dispersion of colloids incurs some corrections to the original analysis by Taylor. The modifications arise when these are comparable in size to plate separation [18], namely when $\lambda = \frac{a_c}{a_p}$ becomes appreciable. The colloids sample smaller portions of the Poiseuille velocity distribution as the distance their centre can approach the walls is limited by their own radius. This excluded region ensures that, on average, colloids travel through the capillary faster than the solvent. Colloids of smaller sizes are also expected to travel slower than larger ones as they can get closer to the boundaries and sample the lower velocities. This size exclusion phenomenon can used to analyse the size of colloidal particles (hydrodynamic chromatography[19]).

Here, we follow the argument of Brenner & Edwards in three dimensions, and we assume that the colloids have the same velocity as the fluid. Then, their average velocity is given by

$$u_c = \frac{3}{2}\frac{\bar{u}}{a_p - a_c}\int_0^{a_p - a_c}\left(1 - \frac{y^2}{a_p^2}\right)dy = \frac{3}{2}\bar{u}\left(\frac{2}{3} + \frac{2}{3}\lambda - \frac{1}{3}\lambda^2\right). \tag{113}$$

For infinitely small colloidal particles, $\lambda = 0$ and $u_c = \bar{u}$ while for particles the size of the channel, $\lambda = 1$ and $u_c = \frac{3}{2}\bar{u}$.

If we redo the derivation of the previous section (6.2.1) taking into account the new boundary conditions then, we find

$$D^* = \frac{2a_c^2\bar{u}^2}{105D}\left(1 - 2.5\lambda + 0.75\lambda^2 + o(\lambda^3)\right). \tag{114}$$

The radial dispersion of the colloids is now effectively reduced as they are unable to sample the higher velocity gradients near the edges, effectively reducing the radial dispersivity, thus leading to a lower value of the Taylor dispersion coefficient.

Through their moment analysis, Brenner & Gaydos[20] found that, in three dimensions, the presence of walls introduced corrections to the first order in λ. The extra terms reduced all the numerical coefficients in in the three dimensional expression of the dispersivity obtained when considering 'excluded region' effects alone. Boundaries therefore reduce the dispersity further.

No study of this problem has been reported in two dimensions. In future simulations, we will try to measure the effect of the wall in three dimensions in order to approximate this contribution.

7.1 Simulation and Preliminary Results

To test Taylor diffusion, and the corrections due to the excluded regions and the wall effects, we performed preliminary simulations of colloidal particles undergoing Taylor diffusion. The simulations were performed in two dimensions, for SRD particles with number density $\gamma = 5$ between parallel plates bounded separated by a distance $h = 32$. The colloids were assumed to be disk like particles of radius $a_c = 2.15a_0$, such that $\lambda \approx 0.13$.

Simulations of Taylor diffusion were run for 24 closely packed colloidal particles at pipe Peclet number $Pe \approx 17$. The runs were carried out in channel of width $h = 32$ ($\lambda \approx 0.13$). The solvent particles were subjected to an external field $g = 0.0004$ along the length of the channel. We measured the resulting mean velocity of the colloids as $5.4 * 10^{-2}$. The mean square displacement with respect to the frame moving at the mean speed along the x-direction was then calculated from

$$W(t) = \frac{1}{N}\sum_{i}^{N}\langle([x_i(t) - x_{com}(t)])^2\rangle, \tag{115}$$

where x_i denotes the x-coordinate of each particles, and x_{com} the position of the centre of mass of the particles at time t. We for simplicity, we shall now refer to this relative average mean square displacement as the m.s.d. The results are shown in Fig.7.

From the m.s.d of the colloids simulated in SRD, we calculated the effective dispersion coefficient of the particles in the channel and found it to be $D \approx 0.22$. The Taylor diffusion coefficient calculated using his original arguments was found to be $D \approx 0.87$ and implementing the 'excluded region' corrections made by Brenner & Edwards yielded a value $D \approx 0.57$ for the dispersion coefficient.

As expected, for finite size particles the Brenner correction gives a slightly better estimate of the motion of the particles although there remains a significant discrepancy between the value given by the correction and the one obtained by simulation. We believe the discrepancy to be due to several factors. Firstly, we have not included any correction terms in λ on account of the walls, which would yield a lower value of D. Furthermore, we have not taken density effects into consideration. As the colloids are closely packed together, hydrodynamic effects will ensue leading to further deviations. Finally, the higher order contributions more important in two dimensions, as we have seen in the case of the diverging diffusion constant in the bulk. We will duly address all these issues in prospective studies.

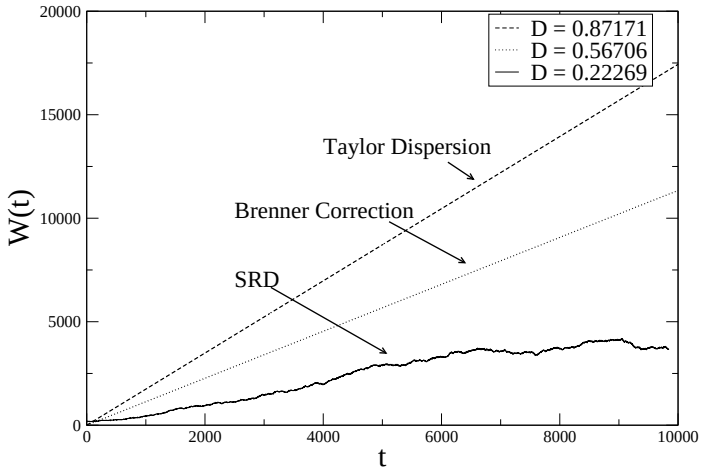

Figure 8: m.s.d of colloidal disk like particles undergoing Taylor diffusion with $\lambda \approx 0.13$ for pipe Peclet number $Pe \approx 17$. The solid curve shows the m.s.d averaged over 24 colloidal particles obtained using SRD. The dashed line corresponds to the theoretical m.s.d of a solute particle as originally predicted by Taylor. The dotted line shows the m.s.d with the 'excluded region' corrections as forecast by Brenner & Edwards.

7.2 Outlook

As previously stated, colloids of different sizes flowing between plates are expected to separate because they sample different ranges of the Poiseuille distribution. For the separation to become apparent, λ should be large enough so that the 'excluded region' correction becomes relevant. If the colloids are too large however, they might have trouble getting past each other, which might may well lead to other corrections.

The derivation of the corrections induced by the channel have been carried out to evaluate the perturbation of the boundaries on the diffusion of colloids. The analysis does not include however the perturbations the colloid itself would induce on the flow. In other words, we have somewhat naïvely assumed so that fluid passes through the colloid particle freely. For large enough colloids, or large enough density of colloids, we would expect their contribution to become more apparent. Will the profile still maintain a Poiseuille distribution in such cases?

The 'excluded region' property of colloid dynamics can also be extended to polymers flowing in narrow channels. The analysis would be less trivial however as polymers can change their shape with the flow.

8 The Limit of 1-D Diffusion: Single File diffusion

In this section, we turn our attention to the motion of colloids in the limit $\lambda \sim 1$, i.e to the limit of one dimensional or single file diffusion.

Single file diffusion (SFD) refers to the-one dimensional motion of particles in channels that are so narrow that mutual passage is excluded. The sequence of the particles remains unchanged and diffusion of any particle depends on the collective motion of neighbouring particles in the same direction. This dependence leads to anomalous (non-Fickian) diffusion in the long time limit for over damped systems. In such systems, particles no longer diffuse in the normal sense but with a $\langle x^2 \rangle \sim t^{1/2}$ dependence of the mean square displacement upon time.

Moreover, if the channel is filled with fluid, the motion of the particles becomes correlated on even more rapidly. As they move through the liquid, they create a flow field that affects the velocities of the particles in the vicinity. Consequently, the motion becomes correlated on a timescale shorter than the direct collision between neighboring particles. On that account, we define the following time scales; the direct interaction time t_I which is time it takes adjacent particles to interact via collisions and the hydrodynamic interaction time t_H which refers to the time it takes a particle to feel its nearest neighbour via hydrodynamic coupling.

The long time behaviour ($t \gg t_I$) induced by the correlated motion has been predicted for infinitely long systems to be[21, 22]

$$\langle x^2 \rangle = F\sqrt{t} \tag{116}$$

where F is the SFD mobility.

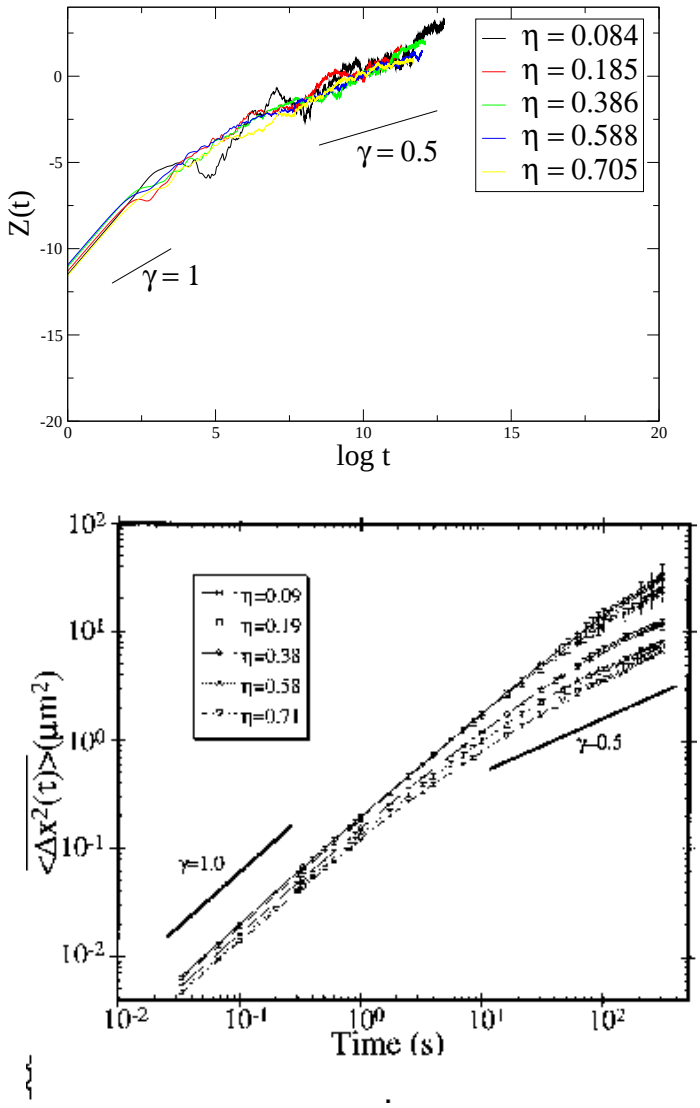

Figure 9: Comparison of the temporal evolution of the mean square displacement at different η, obtained by simulation (top) and experiment (bottom[26]) with particle/channel ratio $\lambda \approx 0.53$ in both cases.

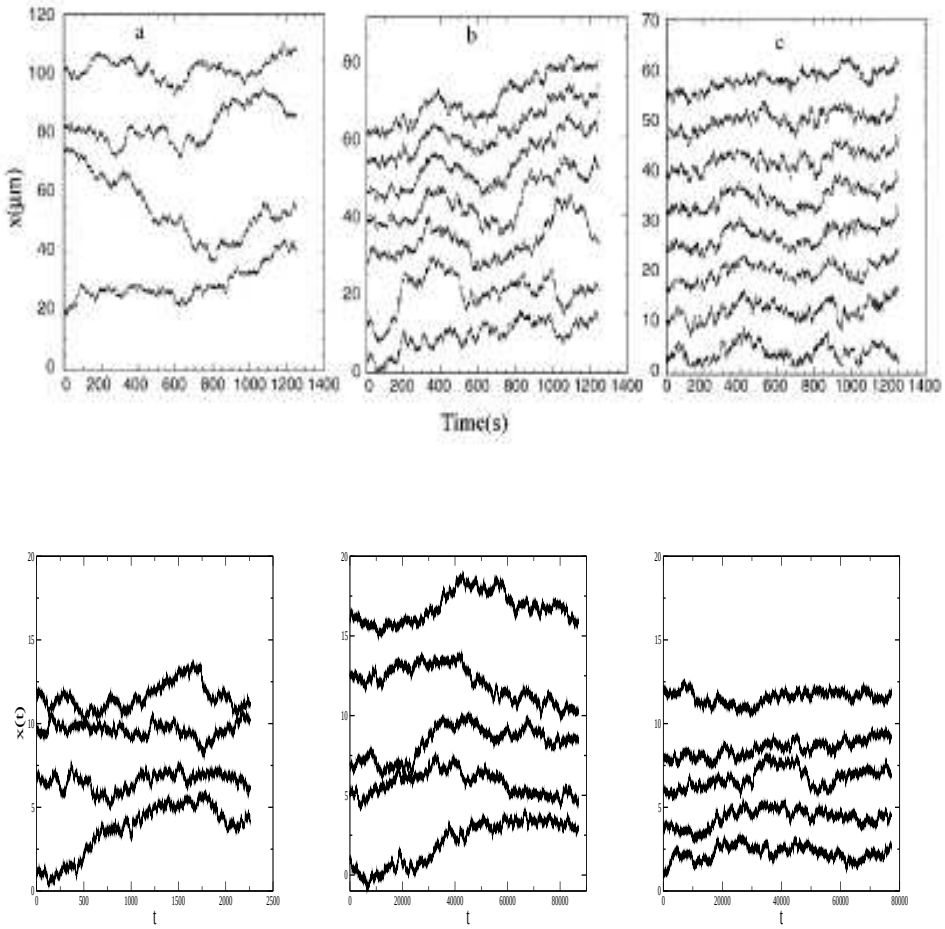

Figure 10: Comparison of the dependent trajectories $x(t)$ for neighbouring spheres for $\eta = 0.09, 0.38$ and 0.71 respectively. Experimental results[26] are plotted in the top graph, and the simulation runs in the bottom plots

8.1 Experimental Review

Several experimental studies have been carried out to investigate hydrodynamic coupling in SFD. Lutz*et.al.*[28] performed an experiment which covered both regimes in order to compare the particle mobility obtained by short time measurements with the long time approximation predicted by theory. The experiments were performed with colloidal particles, and, in contrast to previous SFD studies, the particles were confined to a 1 dimensional geometry by using scanned optical tweezers in order to avoid any hydrodynamic wall effects. Their experimental setup consisted of a silica glass cuvette with $200\mu m$ spacing filled with a highly diluted aqueous suspension of sulphate-terminated polystyrene particles of diameter $2.9\mu m$.

The particle trajectories were recorded for several hours and the mean square displacement was calculated from $Z(t) = \frac{1}{N}\sum_i^N \langle([x_i(t) - x_i(0)])^2\rangle$. $Z(t)$ was then plotted as a function of $t^{1/2}$ and by fitting the data with (116), the mobility was obtained. This was only carried out however for large times where the diffusion was no longer linear. They found good agreement between the data and the theoretical predictions.

The particle displacement distribution function is defined as the conditional probability of finding a particle at position x after time t and is given by

$$P(x,t) = \frac{1}{\sqrt{4\pi F t^{1/2}}} e^{-x^2/4Ft^{1/2}}. \tag{117}$$

Measurements were taken at different times, all greater that t_I and the data was found to be in good agreement with (117). Rescaling the data by $t^{1/4}$ also led to all the curves collapsing to a single master curve.

Lin *et.al.*[26] studied the diffusive behaviour of silica colloidal spheres suspended in water ($a_c \sim 1.58\mu m, \rho = 2g/cm^3$) and confined in long narrow grooves 2 mm long and $3\mu m$ wide and deep. The colloids were slightly charged resulting in slightly attractive pair potential and the system was equilibrated for 6 hours before any measurements were taken. (at $T = 24C$). Using video microscopy they were able to locate the centre of the spheres along the groove and the trajectories were extracted from a sequence of digitised images. Measurements were made at five different packing fraction $\eta = Na_c/L$ where L is the length of the groove in the field of view ($L = 106\mu m$).

They found that in the time regime shorter than the hydrodynamic interaction time, the system underwent normal diffusion. For larger times, still smaller than the direct interaction time, the motion of the spheres was dictated by hydrodynamic interactions. At high enough packing fraction ($\eta > 0.39$) the spheres separated into clusters and moved in synchrony within each cluster. The number of spheres in a cluster also increased as a function of packing fraction. They further constructed a same time pair correlation function (for the four nearest neighbours only). The correlation increased at higher packing fractions as expected. At low packing fractions the correlation to the furthest neighbour was negligible while the was not the case at higher ($\eta = 0.71$).

8.2 Preliminary Results and Further Work

Simulations were performed in two dimensions for colloids of radius $a_c = 2.15a_0$ in a channel of width $a_p = 8a_0$ (such that $\lambda = 0.5375$) for several packing fractions, as observed in experiments[26]. Preliminary results show agreement with the results found by Lin*et.al*. Fig.8 shows that SRD captures the long time diffusive behaviour of the particles for the different packing fractions. Fig.9 shows the correlation between neighboring particles that becomes more pronounced at higher densities.

Further simulations will be carried out to calculated the exact SFD mobilities and the values will be compared to those predicted by theory[21] and found in experiment[28].The precise nature of the correlation behaviour can be better understood by constructing more thorough temporal and spatial velocity correlation functions for the motion of the spheres. This would provide a further test of the apparent density dependence on the size of the particle clusters reported by Lin*et.al*. We can also add flow in the channel and study the system to see if the colloids will behave differently.

9 Laning at High Reynolds Number: Experimental Review

Particles flowing in pipes at finite Reynolds number have been observed to form trains (groups of three or more particles) aligned in the direction of the flow. The trains (sometimes of up to 40 particles) are usually located at the Segré-Silberberg equilibrium position, typically located at a distance $r = 0.6R$ from the centre of the pipe, and move closer to the walls at higher Reynolds numbers. Below is a detailed account of an experiment carried out by Matas *et al.* [29].

Two sets of polystyrene spheres with mean diameters $d = 425 \pm 25\mu m$ and $d = 825 \pm 25\mu m$ were added to a mixture of water (around 78%) and glycerol (around 22%) such that the density formed by the fluid ρ_f matched that of the particles ($\rho_p = 1.05 g/cm^3$). The solutions were kept at temperature $T = 25^o C$ such that their viscosity remained between $\rho = 1.45 - 1.55 cP$. They were then allowed to flow through two horizontal glass tubes of length $L = 26m$ and diameters $D = 8mm$ and $D = 14mm$ such that measurements could be made for $D/d = 33$ and 17 in the larger tube and $D/d = 19$ with the smaller particles in the smaller tube. Measurements were made at a distance of $1.8m$ from the tube entrance to ensure a fully developed Poiseuille flow had been attained. Measurements were made for values of the pipe-scale Reynolds number $Re = \rho_f UD/\nu$ ranging from $100 \leq Re \leq 2400$, with U the mean axial velocity. All experiments were carried out at particle packing fractions of $\phi = 0.17\%$, 0.06% and 0.24% for $D/d = 33$, 17 and 19 respectively. Any correlation between packing the fraction and laning of particles was not investigated as visualisation became increasingly difficult at higher concentrations.

Particles began to form visible trains aligned in the direction of the flow at

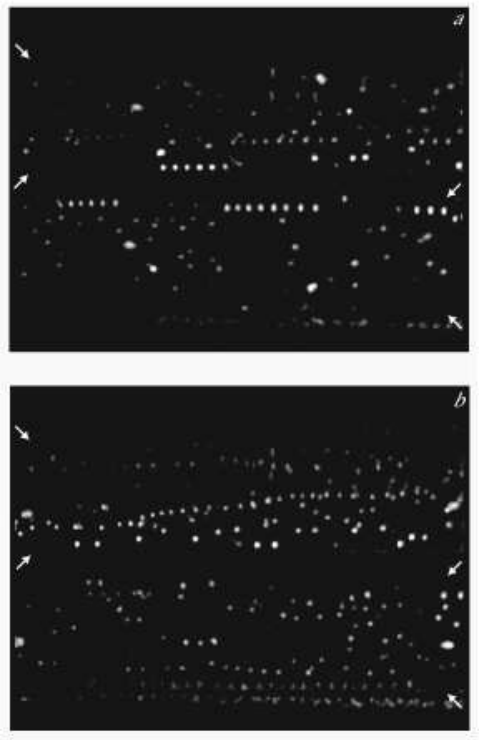

Figure 11: Photograph reproduced from[29]. The picture shows trains trains in the pipe from two perspectives for D/d=19. sad Re=600 (in this photograph, the trains are located on the top of the tube and preferentially in the back), (b) Re=1120 (in this photograph, one observes a very long train having an angle relative to flow). The arrows indicate the walls of the tube from the two perspectives.

$Re \geq 100$. Some trains were also observed to be at an angle to the x-axis of the pipe. The number of particles observed in trains was normalised by the packing fraction and the results showed that as Re became larger the amount of particles in trains increased to a maximum before decreasing. Maxima were reached for $D/d = 17$ and 19 at $Re \sim 700$ and at $Re \sim 950$ for $D/d = 33$. A higher percentage of small particles were found to be in trains (14% for $D/d = 19$ and 8% for $D/d = 17$ at $Re \sim 700$) than larger ones (4% at $Re \sim 950$). It was also found that the percentage of particles in a given train generally decreased with the size of the train. In other words longer size trains were less probable that shorter ones.

The mean surface separation, normalised by the particle separation l/d was found to depend on the particle Reynolds number $Re_p = Re(d/D)^2$. Re_p describes how fluid flows around a given particle. Results showed that l/d decreased for increasing Re but always remained significantly larger for $D/d = 33$. On the other hand, when results were plotted for Re_p the data was found to collapse to a single curve, suggesting that interactions between particles within trains are indeed controlled by Re_p, and particles gathered closer together for increasing Re_p.

Numerical solutions of the flow equations have revealed that the regions of closed streamlines around the particles, predicted for $Re_p = 0$ rapidly collapse with increasing Re_p. The collapsing streamlines give birth to a region of reversed flow, with fluid approaching and receding on each side along the mid-plane of the particle. The fluid is prevented from returning towards the particle by the pipe walls. Furthermore, laning only occurs along the mid-plane, so it seems that flow reversal entices this phenomenon. Solutions for $Re_p = 10$ compares with the highest Re_p studied by Matas *et al.*. Further analysis revealed that the boundary of the reversing streamline grew closer to the particle with increasing Re_p. This relates to particles gathering closer together for higher Re_p as observed by Matas *et al.* Zones of reversed flow were also seen to extend out of the shear plane in the direction of the vorticity, resulting in the formation of angles trains. This was also observed by Matas *et al.* The process of train formation is very much similar to drafting in suspensions except that in the latter case, the particles will kiss, tumble and separate thereafter. Some experiments have revealed however that in thin fluidised beds at $22 \leq Re \leq 43$ particles were seen to form steady arrangements of three or four where each sphere would settle in the shear field of the next.

When the Reynolds number is increased to $Re \geq 600$, the particles are seen to migrate from the Segré-Silberberg annulus to a new annulus which forms closer to the centre of the pipe. No trains are formed on the new annulus, possibly due to the fact that it is broader and thus particles remain too far apart. This accounts for the maxima attained by the amount of particles in trains stated earlier.

In summary, Matas *et al.* have investigated the dependence of lane formation of particles upon the Reynolds number in pipe flow. They have seen that particles will form trains along the Segré-Silberberg annulus, which drifts towards the wall of the pipe for increasing Re. The arrangement of the particles however depends on Re_p which determines the nature of the flow around the particle. Some of these results could be useful for colloids flowing in a pipe. It might provide a convenient

way of aggregating colloids, or at least ordering them in flow. Adjusting the flow properties helps determine the arrangement and position of particle trains. As fluid flows faster in the centre of the tube, the flow properties can be adjusted in order to control the position of the train within the tube, slowing it down or speeding it up.

We would like to try and reproduce these experiments with SRD. However, at present, we have not yet been able to reach the desired Reynolds numbers while maintaining a low enough Mach number.

References

[1] D.J. Acheson: *Elementary Fluid Dynamics*, Oxford University Press (1990)

[2] C.W. Oseen: *hydrodynamik*, Leipzig: Akademische Verlag (1997)

[3] J. Happel, H. Brenner: *Low Reynolds Number Hydrodynamics* Martinus Nijhoff Publishers (1983)

[4] J.R. Lister: *Slow viscous flow*, University of Cambridge, Lecture Notes (2004)

[5] A. Malevanets, R. Kapral: *Mesoscopic model for solvent dynamics*, J. Chem. Phys **110** 8605 (1999)

[6] N. Kikuchi, C.M. Pooley, J.F. Ryder, J.M. Yeomans: *Transport coefficients of a mesoscopic fluid dynamics model*, J. Chem. Phys. **119** 6388 (2003)

[7] A.A. Louis, E. Allahyarov, H. Löwen, R. Roth *Effective forces in colloidal mixtures: From depletion attraction to accumulation repulsion* Phys. Rev. E **65** 061407 (2002)

[8] R.A.L. Jones: *Soft Condensed Matter*, Oxford University Press (2002)

[9] K.A. Dill, S. Bromberg *Molecular Driving Forces, Statistical Thermodynamics in Chemistry and Biology* Garland Science (2003)

[10] B. J. Alder, T. E. Wainwright: *Decay of the Velocity Autocorrelation Function*, Phys. Rev. A **1** 18 (1970)

[11] L.Bocquet, J-L. Barrat: *Decay of the Velocity Autocorrelation Function*, J. Phys. Condens. Matter **8** 9297 (1996)

[12] M.H.J. Hagen, I. Pagonabarraga, C.P. Lowe, D. Frenkel: *Algebraic decay of velocity fluctuations in a confined fluid*, Phys. Rev. Lett **78** 3785 (1997)

[13] G.I. Taylor: *Dispersion of soluble matter in solvent flowing slowly through a tube*, Proc. Roy. Soc. **A219** 186 (1953)

[14] T.M Squires, S.R. Quake: *Microfluidics: Fluid Physics at the Nanoliter Scale*, (2004)

[15] R.F. Probstein: *Physicochemical Hydrodynamics*, Wiley and Sons (1994)

[16] G.I Taylor: *Conditions under which dispersion of a solute in a stream of solvent can be used to measure molecular diffusion*, Proc. Roy. Soc. **A225** 473 (1954)

[17] R. Aris: *On the dispersion of a solute in a fluid flowing through a tube* Proc. Roy. Soc. **A235** 67

[18] H. Brenner, D.A. Edwards: *Macrotransport Processes*, Butterworth-Heinemann, Boston (1993)

[19] A.J. McHugh: *Hydrodynamic Chromatography. In 'Size Exclusion Chromatography'* B.J. Hunt and S.R. Holding. New York: Chapman and Hall.

[20] H. Brenner, L.J. Gaydos: *The constrained brownian movement of spherical particles in cylindrical pores of comparable radius*, J. Coll and Interf. Sci. **58** 313 (1976)

[21] M. Kollmann: *Single file diffusion of atomic and colloidal systems:asymptotic laws*, Phys. Rev. Lett. **90** 180602 (2003)

[22] P.M. Richards: *Theory of one-dimensional hopping conductivity and diffusion*, Phys. Rev. B **16** 1393 (1997)

[23] X. Xu, S.A. Rice: *Influence of hydrodynamic coupling on the density dependence of quasi one dimensional diffusion*, J. Chem. Phys. **122** 024907 (2005)

[24] B. Lin, J. Yu, S.A Rice: *Direct measurements of constrained Brownian motion of an isolated sphere between two walls*, Phys. Rev. E **62** 3909 (2000)

[25] B. Cui, H. Diamant, B. Lin: *Screened hydrodynamic interaction in a narrow channel*, (2003)

[26] B. Lin, B. Cui, J. Lee, J. Yu: *Hydrodynamic coupling in diffusion of quasi one dimensional Brownian particles*, Europhys. Lett. **57** 724 (2002)

[27] Q. Wei, C. Bechinger, P. Leiderer: *Single file diffusion of colloids in one dimensional channels*, Science **287** 625 (2000)

[28] C. Lutz, M. Kollmann, P. Leiderer, C. Bechinger: *Diffusion of colloids in one dimensional channels*, J. Phys. : Cond. Matt **16** 4075

[29] J.P. Matas, V. Glezer, E. Guazzelli, J.F. Morris: *Trains of particles in finite Reynolds number pipe flow*, Phys. Fluids **16** 11 (2004)

A Appendix

A.1 Proof that Φ' is harmonic

We wish to prove the following relation

$$\nabla^2\Phi' = \nabla^2(\Phi + \nabla\phi) = 0 \text{ i.e. } \nabla^2\nabla\phi = \nabla\nabla^2\phi = 0 \tag{118}$$

for a harmonic scalar $\phi(r)$ in spherical coordinates. From the definition

$$\nabla^2\phi = \frac{1}{r^2}\frac{\partial}{\partial r}\left(r^2\frac{\partial\phi}{\partial r}\right) = \frac{2}{r}\frac{\partial\phi}{\partial r} + \frac{\partial^2\phi}{\partial r^2} = 0 \tag{119}$$

and so

$$\nabla\nabla^2\phi = r\frac{\partial}{\partial r}\left(\frac{2}{r}\frac{\partial\phi}{\partial r}+\frac{\partial^2\phi}{\partial r^2}\right) = -\frac{2}{r}\frac{\partial\phi}{\partial r}+2\frac{\partial^2\phi}{\partial r^2}+r\frac{\partial^3\phi}{\partial r^3} = 0. \tag{120}$$

From the definition it also follows that

$$\nabla^2\nabla\phi = \frac{1}{r^2}\frac{\partial}{\partial r}\left(r^2\frac{\partial}{\partial r}\left(r\frac{\partial\phi}{\partial r}\right)\right) = \frac{2}{r}\frac{\partial\phi}{\partial r}+4\frac{\partial^2\phi}{\partial r^2}+r\frac{\partial^3\phi}{\partial r^3} \tag{121}$$

and

$$\nabla^2\nabla\phi - \nabla\nabla^2\phi = \frac{4}{r}\frac{\partial\phi}{\partial r}+2\frac{\partial^2\phi}{\partial r^2} = 2\underbrace{\left(\frac{2}{r}\frac{\partial\phi}{\partial r}+\frac{\partial^2\phi}{\partial r^2}\right)}_{0} = 0. \tag{122}$$

thus $\nabla^2\nabla\phi = \nabla\nabla^2\phi$, i.e. the operators commute for a harmonic scalar ϕ in spherical coordinates.